STAT5 is a key regulator in NK cells and acts as molecular switch from tumor surveillance to tumor promotion

Running title: NK cells as tumor promoters

Key words: NK cells; STAT5; NK-cell mediated tumor surveillance; VEGF-A, tumor promotion;

Dagmar Gotthardt,[1] Eva M. Putz,[1,δ] Eva Grundschober[1], Michaela Prchal-Murphy[1], Elisabeth Straka,[1] Petra Kudweis,[1] Gerwin Heller[2,3], Zsuzsanna Bago-Horvath[4], , Agnieszka Witalisz-Siepracka[5], Abbarna A. Cumaraswamy[7], Patrick T. Gunning[7], Birgit Strobl[5], Mathias Müller[5], Richard Moriggl[5,6], Christian Stockmann[8], Veronika Sexl[1]

[1]Institute of Pharmacology and Toxicology, Department for Biomedical Sciences, University of Veterinary Medicine Vienna, A-1210 Vienna, Austria

[δ]current affiliation: Immunology in Cancer and Infection Laboratory, QIMR Berghofer Medical Research Institute, Herston, Queensland 4006, Australia

[2]Department of Medicine I, Clinical Division of Oncology, Medical University of Vienna, Vienna, Austria

[3]Comprehensive Cancer Center, Medical University of Vienna, Vienna, Austria

[4]Clinical Institute of Pathology, Medical University of Vienna (MUV), Waehringer Gürtel 18-20, Vienna 1090, Austria

[5]Institute of Animal Breeding and Genetics; Department for Biomedical Sciences, University of Veterinary Medicine; Vienna, Austria, A-1210 Vienna, Austria

[6]Ludwig Boltzmann Institute for Cancer Research (LBI-CR), Vienna 1090, Austria

[7]Department of Chemistry, University of Toronto Mississauga, Mississauga, Ontario L5L 1C6, Canada

[8]PARCC Paris - Centre de recherche Cardiovasculaire à l'HEGP Inserm - UMR 970, 75015 Paris, France

Correspondence

Veronika Sexl
Institute of Pharmacology and Toxicology,
University of Veterinary Medicine Vienna,
Veterinaerplatz 1, A-1210 Vienna, Austria
Phone number: 0043 1 25077 2910
Fax: 0043 1 25077 2990
Email: veronika.sexl@vetmeduni.ac.at

Conflict of interest disclosure

The authors declare no potential conflicts of interest.

Abstract

Natural Killer (NK) cells are tightly regulated by the JAK-STAT signaling pathway and cannot survive in the absence of STAT5. We now report that STAT5-deficient NK cells can be rescued by overexpression of Bcl-2. Our experiments define STAT5 as a master regulator of NK-cell proliferation and lytic functions. While NK cells are generally responsible for killing tumor cells, the rescued STAT5-deficient NK cells promote tumor formation by producing enhanced levels of the angiogenic factor VEGF-A. The importance of VEGF-A produced by NK cells was verified by experiments with a conditional knock-out of Vegf-A in NK cells. We show that STAT5 normally represses the transcription of VEGF-A in NK cells, both in the mouse and in the human. The findings reveal that STAT5-directed therapies may have negative effects: in addition to impairing NK cell-mediated tumor surveillance they may even promote tumor growth by enhancing angiogenesis.

Statement of Significance

The importance of the immune system in effective cancer treatment is widely recognized. We show that the new signal-interceptors targeting the JAK- STAT5 pathway may have dangerous side effects that must be taken into account in clinical trials: inhibiting JAK/Stat5 has the potential to promote tumor growth by enhancing NK cell-mediated angiogenesis.

Introduction

Natural Killer (NK) cells are innate lymphocytes that develop from a common lymphoid progenitor in the bone marrow (1). They represent the first line of defense against infected, stressed and malignant cells. Recent evidence has assigned distinct features and functions to tissue-specific NK cells (2). NK cells have organ-specific properties such as distinct profiles of receptor expression or cytokine production (3). Uterine NK cells secrete high levels of VEGF-A and are involved in placental vascularization. The physiological functions of other organ-specific NK-cell subsets are less well understood (4).

All aspects of NK-cell development are regulated by cytokines, their downstream signaling pathways and transcriptional regulators. These include key cytokines such as IL-2, IL-12, IL-15, IL-18 and IL-21 (5), most of which signal via the common γ chain (5) and activate the JAK-STAT pathway (6). JAK kinases (JAK1-3 and TYK2) bind to cytokine receptors and are activated by ligand/receptor binding. The activated kinase phosphorylates STAT transcription factors (STAT1-STAT6) (6,7).

Consistent with its function as the major STAT protein downstream of IL-7, IL-2 and IL-15, STAT5 is absolutely essential for conventional NK-cell development and survival; *Stat5*$^{\Delta/\Delta}$*Ncr1*-iCre^{Tg} mice lack NK cells (8). It is also important for lymphoid cell development (9): STAT5 is constitutively active in a plethora of lymphoid malignancies (10). Recent studies have described somatic *Stat5b* mutations as active drivers of lymphoid malignancies (11,12) and considerable efforts are under way to develop STAT5 inhibitors. Such inhibitors will not only target malignant hematopoietic cells but will also have severe consequences for immune functions that depend on the activation of STAT5 by cytokines. A precise understanding of the detailed function of STAT5 in immune cells is required to predict the potential side effects of a STAT5-directed therapy.

We now provide the first evidence that STAT5 is more than a master regulator of NK cell survival, proliferation and cytotoxicity: it also inhibits NK cell-mediated tumor angiogenesis by directly suppressing the transcription of the angiogenic factor VEGF-A. This finding forces us to reconsider the potential consequences of STAT5-directed therapies for NK-cell surveilled tumors.

Results

Overexpression of *Bcl-2* rescues survival of STAT5-deficient NK cells

STAT5 regulates the anti-apoptotic genes *Bcl-xl, Bcl-2* and *Mcl-1* in various cell types (13–17). The lack of expression of these genes would explain the almost complete absence of mature NK cells in *Stat5*$^{\Delta/\Delta}$*Ncr1*-iCre^{Tg} mice. We investigated the level of the transcripts of these genes in NK cells derived from heterozygotic *Stat5*$^{\Delta/+}$*Ncr1*-iCre^{Tg} mice. We found about 50% of the wild-type number of mature natural killer cells in the periphery of *Stat5*$^{\Delta/+}$*Ncr1*-iCre^{Tg} mice (Figure 1A), indicative of a gene dosage effect. The reduced levels of *Stat5a* and *Stat5b* are paralleled by decreased levels of *Bcl-xl, Bcl-2* and *Mcl-1* (Figure S1A+B). To investigate the association between STAT5 levels, the expression of anti-apopotic genes and NK-cell survival we crossed *Stat5*$^{\Delta/\Delta}$*Ncr1*-iCre^{Tg} mice - which display a drastic reduction in NKp46^{+} NK cell numbers (8) - to *vav-bcl-2* mice. Expression of the *Bcl-2* transgene rescues STAT5-deficient NK cells; the numbers of CD3^{-}NKp46^{+} cells in the spleen, lymph nodes, liver and lung of *Stat5*$^{\Delta/\Delta}$*Ncr1*-iCre^{Tg}-*vav-bcl-2* mice are comparable to those in *Stat5*$^{fl/fl}$ animals, although they did not reach the levels of *vav-bcl-2* transgenic animals. The overexpression of *Bcl-2* also leads to an increased number of NK cells in the bone marrow in both *Stat5*$^{\Delta/\Delta}$*Ncr1*-iCre^{Tg}-*vav-bcl-2* and *vav-bcl-2* mice (Figure 1B+ S1C).

Q-PCR analysis of IL-2-cultured *Stat5*$^{\Delta/\Delta}$*Ncr1*-iCre^{Tg}-*vav-bcl-2* showed drastically reduced levels of both *Stat5* isoforms in *Stat5*$^{\Delta/\Delta}$*Ncr1*-iCre^{Tg}-*vav-bcl-2* NK cells. The residual STAT5 most likely reflects non-deleting NK cells and "recent deleters", which retain some STAT5 due to the long half-life of the protein (8) (Figure 1C). PCR confirmed that the *Stat5* gene had been deleted in *Stat5*$^{\Delta/\Delta}$*Ncr1*-iCre^{Tg}-*vav-bcl-2* NK cells (Figure S1D). We also found a consistent reduction of *Stat5a* and *Stat5b* levels in *vav-bcl-2* NK cells (Figure 1C) which most likely results from a decreased expression of cytokine receptors in these mice (data not shown). To confirm the rescue of STAT5-deficient NK cells by Bcl-2, we generated *Stat5*$^{fl/fl}$*Mx1*-Cre-*vav-bcl-2* mice, which allow *Stat5* to be deleted conditionally by treatment with Poly (I:C). In contrast to *Stat5*$^{\Delta/\Delta}$*Ncr1*-iCre^{Tg} mice, where deletion only affects late NK-cell stages, *Stat5*$^{fl/fl}$*Mx1*-Cre animals delete *Stat5* in all NK cells irrespective of their developmental stage. In line with our previous observations, deletion of STAT5 in *Stat5*$^{\Delta/\Delta}$*Mx1*-Cre mice resulted in the lack of splenic NK cells, whereas *Stat5*$^{\Delta/\Delta}$*Mx1*-Cre-*vav-bcl-2* animals had comparable numbers of NK cells to *Stat5*$^{fl/fl}$ mice (Figure S1E). Deletion of STAT5 and the levels of Bcl-2 were verified by qPCR and Western blotting (Figure S1F-H). The results confirmed that Bcl-2 expression enables cells to survive the deletion of STAT5.

STAT5 regulates NK cell maturation

NK cell maturation takes place in distinct stages, which can be distinguished by the expression of CD27 and CD11b. NK cells acquire CD27 before they express CD11b. CD27^{+}CD11b^{+} NK cells represent cytotoxic NK cells, which cease to express CD27 to become CD27^{-}CD11b^{+} (18,19). Loss of one allele of *Stat5* results in reduced numbers of CD27^{+}CD11b^{+} NK cells, paralleled by an increase of immature CD27^{-}CD11b^{-}and CD27^{+}CD11b^{-} NK cells (Figure 1D+E). The absence of both Stat5 alleles in *Stat5*$^{\Delta/\Delta}$*Ncr1*-iCre^{Tg}-*vav-bcl-2* mice is associated with the appearance of

highly immature NK cells ($CD27^{-}CD11b^{-}$) (Figure 1D). A similar pattern was observed in *vav-bcl-2* mice, as *Bcl-2* expression stabilizes the immature NK-cell stage (20). NK-cell maturation can be induced by type 1 interferon in *vav-bcl-2* mice, which is blocked by the absence of *Stat5* in *Stat5*$^{\Delta/\Delta}$*Mx1-Cre-vav-bcl-2* mice (Figure 1E). Thus STAT5 is involved in NK-cell maturation; NK cells overexpressing *Bcl-2* do not mature but can be stimulated to do so. The impaired NK-cell maturation in *Stat5*$^{\Delta/+}$*Ncr1*-iCre^{Tg}, *vav-bcl-2* and *Stat5*$^{\Delta/\Delta}$*Ncr1*-iCre^{Tg}-*vav-bcl-2* mice is paralleled by significantly decreased expression of the transcription factor *Id2* (Figure 2A, S2A). It is also characterized by reduced mRNA and protein levels of the T-box transcription factor family members *T-bet* and *Eomes* (Figure 2A, S2B-E), although the results with T-bet did not consistently reach statistical significance (Figure S2B-E).

STAT5 regulates NK cell proliferation and the lytic machinery

STAT5 regulates genes involved in cell-cycle control, including c-myc and D-type cyclins (21,22). To investigate the requirement for STAT5 in NK cell proliferation, we analysed growth curves of purified NK cells maintained in IL-2. While *Stat5*$^{fl/fl}$ and *vav-bcl-2* NK cells proliferate with comparable kinetics, *Stat5*$^{\Delta/\Delta}$*Ncr1*-iCre^{Tg}-*vav-bcl-2* NK cells have a pronounced growth disadvantage (Figure 2B). The reduced proliferative ability of STAT5-deficient NK cells was confirmed *in vivo* using BrdU incorporation (Figure 2C). *Stat5*$^{\Delta/\Delta}$*Ncr1*-iCre^{Tg}-*vav-bcl-2* NK cells displayed reduced expression of cyclin D2 (*Ccnd2*) and c-Myc (*Myc*), prominent regulators of growth and cell-cycle control (Figure 2D). In contrast to proliferation, apoptosis did not appear to be affected by the absence of *Stat5* in *Stat5*$^{\Delta/\Delta}$*Ncr1*-iCre^{Tg}-*vav-bcl-2* NK cells, as revealed by AnnexinV/7-AAD staining (Figure S2F).

NK cells produce high levels of perforin, granzymes and IFN-γ (23). To test whether STAT5 is involved in the regulation of NK-cell cytotoxicity we analysed mRNA and protein levels of

Perforin (*Prf1*), Granzyme A/B (*Grzma/b*) and IFN-γ (*Ifng*). *Stat5*$^{\Delta/\Delta}$*Ncr1*-iCre^{Tg}-*vav-bcl-2* NK cells consistently showed a significant reduction in the levels of all effector molecules (Figure 2E, Figure S3A-C). In line with the reduced STAT5 activation found in non-activated *ex vivo*-derived *vav-bcl-2* NK cells we found a decrease in levels of the effector molecules (Figure 2E and S3A). In contrast, no differences were observed upon activation in interferon-treated cells (Figure S3B+C). *In vitro* cytotoxicity assays confirmed the physiological significance of these observations: NK cells with diminished levels of STAT5 cannot efficiently lyse target cells (Figure 2F). Supporting evidence was provided by adoptive transfer of IL-2-expanded NK cells into *Rag2*$^{-/-}$*gc*$^{-/-}$ mice: in the absence of STAT5 the NK cells were unable to suppress the growth of RMA-S cells (Figure S3D).

Loss of STAT5 in NK cells is associated with a tumor-promoting effect *in vivo*

To study NK cell-mediated tumor surveillance *in vivo*, we injected 5x10^4 B16F10 melanoma cells into the tail vein of *Stat5*$^{fl/fl}$, *Stat5*$^{\Delta/\Delta}$*Ncr1*-iCre^{Tg}, *Stat5*$^{\Delta/\Delta}$*Ncr1*-iCre^{Tg}-*vav-bcl-2* and *vav-bcl-2* mice. Survival (Figure 3A) and tumor nodules in the lung (Figure 3B) were analysed in two independent experiments. Despite the presence of normal numbers of NK cells in *Stat5*$^{\Delta/\Delta}$*Ncr1*-iCre^{Tg}-*vav-bcl-2* mice (Figure 1B), no efficient rejection of the melanoma cells was observed: the onset of disease in *Stat5*$^{\Delta/\Delta}$*Ncr1*-iCre^{Tg}-*vav-bcl-2* mice was as accelerated as in *Stat5*$^{\Delta/\Delta}$*Ncr1*-iCre^{Tg} mice (Figure 3A). The majority of *vav-bcl-2* mice were able to reject the B16F10 cells efficiently, possibly related to the higher numbers of NK cells (Figure 1B). To analyse tumor burden in the lung, mice were again injected with 5x10^4 B16F10 tumor cells and sacrificed after 23 days. Numbers of tumor nodules in *Stat5*$^{\Delta/\Delta}$*Ncr1*-iCre^{Tg}-*vav-bcl-2* mice were similar to those in *Stat5*$^{\Delta/\Delta}$*Ncr1*-iCre^{Tg} mice (Figure 3B). The presence of NK cells expressing high levels of Bcl-2 but lacking STAT5 was not sufficient to control tumor growth (Figure 3A+B).

NK cells also play a prominent role in the surveillance of hematopoietic tumors (24–26). We subcutaneously (s.c.) injected the hematopoietic cell line RMA-S and *v-abl* transformed cells into *Stat5*$^{\Delta/\Delta}$*Ncr1*-iCre^{Tg}-*vav-bcl-2* mice. Both experiments had to be terminated after about a week (day 6 for *v-abl* and day 9 for RMA-S cells) as tumors developed extremely rapidly in *Stat5*$^{\Delta/\Delta}$*Ncr1*-iCre^{Tg}-*vav-bcl-2* mice. The accelerated tumor growth in *Stat5*$^{\Delta/\Delta}$*Ncr1*-iCre^{Tg}-*vav-bcl-2* mice gave rise to a high tumor mass, while *Stat5*$^{\Delta/\Delta}$*Ncr1*-iCre^{Tg} mice had small tumors at the same time point (Figure 3C-E for *v-abl*, S4A+B for RMA-S). We reasoned that at this early tumor stage the residual "non-deleting" NK cells in *Stat5*$^{\Delta/\Delta}$*Ncr1*-iCre^{Tg} mice were able to control tumor growth. Importantly, we did see significant differences between *Stat5*$^{fl/fl}$ and *Stat5*$^{\Delta/\Delta}$*Ncr1*-iCre^{Tg} mice under challenge with a higher number of cells when the tumor burden was examined at later stages, confirming the critical role of NK cells (Figure S4C). Despite the presence of equal numbers of NK cells in *Stat5*$^{\Delta/\Delta}$*Ncr1*-iCre^{Tg}-*vav-bcl-2* and *Stat5*$^{fl/fl}$ mice, a tumor-promoting effect was only observed in the presence of STAT5-deficient NK cells; the effect could be reversed by depletion of NK cells (Figure 3F, S4D).

This result suggests that NK cells that survive the loss of STAT5 are able to accelerate tumor formation and that STAT5 acts as a molecular switch in NK cells, regulating tumor suppression and tumor promotion. Irrespective of the ability of NK cells to recognize and eradicate tumor cells, lowering STAT5 levels in NK cells will exacerbate tumor growth. We tested this interpretation in a tumor model that is not subject to immune surveillance by NK cells (25,27). Upon s.c. injection, RMA cells induced tumor development to a comparable extent and with similar kinetics in *Stat5*$^{\Delta/\Delta}$*Ncr1*-iCre^{Tg}, *Stat5*$^{fl/fl}$ and *vav-bcl-2* animals. Tumor growth was significantly accelerated in *Stat5*$^{\Delta/\Delta}$*Ncr1*-iCre^{Tg}-*vav-bcl-2* mice (Figure 4A+B). To verify that the tumor-promoting potential resides within the *Stat5*-deficient NK cells, we depleted NK cells

using an anti-NK1.1 antibody in *Stat5*$^{\Delta/\Delta}$*Ncr1*-iCre^{Tg}-*vav-bcl-2* mice and controls. NK-cell depletion abrogated the tumor-promoting potential and *Stat5*$^{\Delta/\Delta}$*Ncr1*-iCre^{Tg}-*vav-bcl-2* animals had a tumor burden comparable to that of *Stat5*$^{fl/fl}$ mice (Figure 4C). This clearly demonstrates that the NK cells themselves are responsible for the enhanced tumor progression.

NK cells secrete VEGF-A and promote endothelial cell growth

The development of subcutaneous tumors relies on the formation of new blood vessels (28). CD31 is a marker for angiogenesis and we found significantly more CD31^{+} cells in tumors derived from *Stat5*$^{\Delta/\Delta}$*Ncr1*-iCre^{Tg}-*vav-bcl-2* mice (Figure S4E). VEGF-A plays a key part in tumor angiogenesis. We detected VEGF-A expression in NK cells under basal conditions. Experiments with IL-2-expanded NK cells showed that *Stat5*$^{\Delta/\Delta}$*Ncr1*-iCre^{Tg}-*vav-bcl-2* NK cells have significantly enhanced levels of *Vegf-A* mRNA compared to *Stat5*$^{fl/fl}$ *and vav-bcl-2* cells (Figure 4D). Comparable results were obtained in *Stat5*$^{\Delta/\Delta}$*Mx1*-Cre-*vav-bcl-2* NK cells: levels of *Vegf-A* mRNA were significantly increased upon *Stat5* deletion (Figure S5A). To test the physiological significance of VEGF-A produced by NK cells we embedded endothelial cells in a 3D collagen matrix and enriched it with the supernatant of *in vitro*-expanded NK cells. After 24 hours we observed basal sprouting with the supernatant of *Stat5*$^{fl/fl}$ and *vav-bcl-2* NK cells in parallel with basal VEGF-A production, whereas the supernatant of *Stat5*$^{\Delta/\Delta}$*Ncr1*-iCre^{Tg}-*vav-bcl-2* NK cells drastically increased the average sprout number as well as the cumulative sprouting length (Figure 4E-F). A neutralizing VEGF-A antibody prevented the increased sprouting (Figure S5B). The pro-angiogenic effect was confirmed in assays with aortic rings embedded in 3D collagen matrices. Supernatants of *Stat5*$^{fl/fl}$ and *vav-bcl-2* NK cells induced a certain level of sprouting but addition of supernatant from *Stat5*$^{\Delta/\Delta}$*Ncr1*-iCre^{Tg}-*vav-bcl-2*-derived NK cells caused significantly enhanced sprouting (Figure S5C). The supernatants of NK cell cultures thus

contain pro-angiogenic factors, which are produced in higher concentrations in the absence of STAT5.

NK cell-derived VEGF-A exerts tumor promoting functions *in vivo*

We have shown that NK cells produce angiogenic factors that trigger endothelial cell sprouting *in vitro* and that the tumor-promoting effect observed in *Stat5*$^{\Delta/\Delta}$*Ncr1*-iCre^{Tg}-*vav-bcl-2* mice correlates with increased tumor angiogenesis. To test the *in vivo* significance of our findings we crossed *Vegf-A*$^{fl/fl}$ mice to *Ncr1*-iCre^{Tg} mice to produce *Vegf-A*$^{\Delta/\Delta}$*Ncr1*-iCre^{Tg} mice, in which the deletion of *Vegf-A* is restricted to NKp46^{+} NK cells. The numbers of NK cells in the periphery (spleen, blood, lymph nodes) were unaffected despite the deletion of *Vegf-A* in splenic *ex vivo*-derived NKp46^{+} NK cells (Figure S6A+B). We found no consistent or significant changes in NK-cell proliferation or maturation (Figure S6C+D). To investigate the role of NK cell-derived VEGF-A in tumor development, we injected *v-abl*$^{+}$ tumor cells s.c. into the flanks of the mice. *Vegf-A*$^{\Delta/\Delta}$*Ncr1*-iCre^{Tg} mice showed a significantly reduced tumor burden (Figure 5A-C). The reduction in tumor angiogenesis was confirmed immune-histochemically: tumors of *Vegf-A*$^{\Delta/\Delta}$*Ncr1*-iCre^{Tg} mice had significantly fewer CD31^{+} cells (Figure 5D). VEGF-A deficient NK cells were not able to efficiently induce sprouting of endothelial spheroids (Figure S6E). The reduced tumor burden was abolished by depletion of NK cells (Figure S6F+G).

To confirm the pro-tumorigenic potential of NK cell-derived VEGF-A, we injected RMA-S cells s.c. into the flanks of mice (Figure S6H). In addition we used a retrovirally induced leukemia model that triggers a slowly and oligoclonally evolving disease that closely reflects the situation in human patients. We injected *Vegf-A*$^{fl/fl}$ and *Vegf-A*$^{\Delta/\Delta}$*Ncr1*-iCre^{Tg} newborn mice with a replication-incompetent ecotropic retrovirus encoding *v-abl*. *Vegf-A*$^{\Delta/\Delta}$*Ncr1*-iCre^{Tg} mice

displayed a significantly increased disease latency and survived longer than *Vegf-A*$^{fl/fl}$ controls (Figure 5E). Consistent with the results in Figure 3A and B, *Vegf-A*$^{fl/fl}$ and *Vegf-A*$^{\Delta/\Delta}$*Ncr1*-iCre^{Tg} mice showed no differences in tumor burden in the B16F10 melanoma model (Figure S6I). This probably stems from the fact that B16F10 melanoma forms multiple small nodules in the lung that require less angiogenesis. In addition the lung is well oxygenized, reducing the need for angiogenesis in evolving small tumors.

Myeloid cells are a source of VEGF-A in the tumor microenvironment (29,30). We found that both myeloid cells and NK cells infiltrate *v-abl*$^{+}$ tumors in comparable numbers between all genotypes (Figure 5F, S7A-C). Although both NK cells and myeloid cells are present around blood vessels, the results of experiments with VEGF-A-deficient NK cells show the *in vivo* significance of NK cell-derived VEGF-A for hematopoietic tumors.

STAT5 regulates VEGF-A production in mice and human

We have shown that loss or absence of STAT5 is associated with increased levels of VEGF-A. To investigate how STAT5 interferes with the production of VEGF-A we stimulated *ex vivo*-derived NK cells with IL-2 or IL-2+IL-15. Both cytokines strongly activate STAT5, accompanied by a decrease in *Vegf-A* mRNA (Figure 6A). STAT5 ChIP analysis of primary NK cells after stimulation showed an increase in STAT5 binding to the *Vegf-A* promoter (Figure 6B). To investigate which cytokines affect STAT5 activation in NK cells, we stimulated IL-2-expanded WT NK cells with IL-6, IL-12, IL-15, IL-18, IL-21, IL-23 or IFN-β. While IL-6 and IL-23 do not alter STAT5 activation, IL-10, IL-12, IL-18, IL-21 and IFN-β lead to a clear downregulation of STAT5-Y694 phosphorylation (Figure 6C). In line with the decreased STAT5 activation, there is a clear increase in *Vegf-A* mRNA levels in NK cells after stimulation with IL-

10, IL-12, IL-18, IL-21 or IFN-β (Figure S8A). STAT5 occurs in two isoforms, STAT5A and STAT5B, which are encoded by adjacent genes and share at least 90% homology. They are generally considered to have highly redundant functions (31) but using NK cells purified from *Stat5a* and *Stat5b* knockout mice we found that the amount of *Vegf-A* mRNA was increased only in the absence of STAT5B (Figure 6D).

Human peripheral blood NK cells are also able to produce *VEGF-A*, with immature $CD16^{-}CD56^{bright}$ NK cells secreting higher levels than mature $CD16^{+}CD56^{+}$ NK cells (4). We FACS-sorted both NK-cell populations from healthy human donors (n=8) and analysed the levels of *STAT5* and *VEGF-A*. We found that $CD16^{-}CD56^{bright}$ NK cells contain high levels of *VEGF-A*, accompanied by low levels of *STAT5A*, *B* and the downstream target *BCL-2* when compared to $CD16^{+}CD56^{+}$ NK cells (Figure 6E, Figure S8B). Within the $CD16^{-}CD56^{bright}$ NK cell population we detected an inverse correlarion between *VEGF-A* and *STAT5B*, the relevant *STAT5* isoform regulating *VEGF-A* (Pearson Correlation: R=0.689, p=0.003 comparing *STAT5A* and *VEGF-A* and R=-0.547, p=0.028 comparing *STAT5B* and *VEGF-A*, Figure S8C). The data were confirmed by a scatter plot and a microarray expression analysis comparing resting and IL-2-activated human NK cells (Figure 6F, Figure S8D). Upon stimulation with IL-2, human NK cells upregulate STAT5 target genes such as *EOMES*, *CCND2* and *CISH*, whereas the expression of *VEGF-A* is reduced (Figure 6F, Figure S8D).

A number of inhibitors of STAT5 and its upstream kinases is currently the subject of pre-clinical investigations and clinical trials. Treatment of murine IL-2-expanded NK cells with a pre-clinical STAT5 inhibitor caused a significant upregulation of *Vegf-A* expression and a clear downregulation of the STAT5 target genes *Bcl-2*, *Mcl-1* and *Cish* (Figure S8E). Treatment of mouse NK cells with Ruxolitinib, an inhibitor of the upstream kinases JAK1/2/3, significantly

increased the levels of *Vegf-A* mRNA (Figure 7A). Treatment of FACS-sorted $CD3^{-}CD56^{+}$ PBMCs with 0.5 µM Ruxolitinib was sufficient to prevent activation of STAT5, as indicated by STAT5-Y694 phosphorylation (Figure 7B). After a three-hour treatment with the inhibitor, human peripheral blood NK cells expressed significantly higher levels of *VEGF-A* (Figure 7C), suggesting that Ruxolitinib not only inhibits STAT5 signaling but also stimulates the secretion of pro-angiogenic factors. This finding is of direct relevance to patients. The effect is observed *in vivo*: Ruxolitinib treatment of *Vegf-A*$^{fl/fl}$ mice subcutaneously injected with *v-abl*$^{+}$ tumor cells gave rise to an increased tumor burden that was not observed in *Vegf-A*$^{\Delta/\Delta}$*Ncr1*-iCre^{Tg} mice (Figure 7D+E). This experiment confirms that Ruxolitinib accelerates tumor progression by enhancing NK-cell-derived VEGF-A expression.

Discussion

We report that STAT5-deficient NK cells are rescued by overexpression of the anti-apoptotic gene *Bcl-2*. This finding enabled us to investigate the functions of STAT5 in NK cells. STAT5 is a key regulator of NK-cell maturation, proliferation and cytotoxicity. Not only does STAT5 regulate the transcription of genes that have been identified as targets in other cell types (*Myc*, *Ccnd2* or *Prf1*) (32), but also it is involved in the regulation of the transcription factors *Eomes* and *Id2*. *Vav-bcl-2* mice show reduced basal levels of STAT5 in non-activated NK cells, together with an impairment of NK-cell maturation and reduced levels of effector molecules, while NK cell proliferation and cytotoxicity are largely unimpaired. Stimulation with cytokines causes maturation, consistent with the idea that the delay in maturation is related to a decreased level of cytokine receptors in non-activated *bcl-2*-transgenic NK cells (data not shown). *Vav-bcl-2* mice

are comparable to wild-type mice in many key functions, such as NK-cell tumor surveillance. In contrast, *Stat5*$^{\Delta/\Delta}$*Ncr1*-iCre^{Tg}-*vav-bcl-2* mice that lack STAT5 in NK cells show severely hampered NK-cell function.

The most striking finding is that NK cells promote tumor formation in the absence of STAT5. We show that wild-type cytotoxic NK cells secrete significant levels of *Vegf-A* and that transcription of *Vegf-A* is suppressed by STAT5, especially by STAT5B. Loss of STAT5 causes increased production of *Vegf-A* in two mouse models. The increased levels of *Vegf-A* promote tumor formation. Experiments with conditional knockout mice have confirmed the significance of the pro-tumorigenic role of NK cell-derived *Vegf-A*: loss of NK cell-derived *Vegf-A* decreases tumor burden while increasing disease latency.

Immune cells such as tumor-associated macrophages promote tumor angiogenesis and lymphangiogenesis (29,30). However, tumor-infiltrating NKp46^{+} NK cells are also found in the surroundings of blood vessels and VEGF-A produced by NK cells enhances the formation of lymphoid tumors. Infiltrating immature NK cells that secrete VEGF-A have been detected in patients with non-small cell lung cancer, breast and colon tumors (33,34). The presence of VEGF-A-producing NK cells is associated with a poor prognosis, showing that NK-cell-derived VEGF-A plays a part in human disease. Which cells are primarily responsible for producing VEGF-A in a particular context presumably depends on the type and stage of the tumor. It is currently unclear whether tumor-associated NK cells and macrophages interact to promote tumor growth and angiogenesis. It will be of great interest to test whether NK cells contribute to the polarization of macrophages.

Depending on the context, NK cells may have either cytotoxic or angiogenic functions. We propose that STAT5 regulates the switch between the two effects. There is ample evidence that tumor-infiltrating NK cells have low cytotoxic potential. It has been speculated that treatment with IL-2 and IL-15 re-activates non-cytotoxic NK cells (35). Our data support the idea: these cytokines signal via STAT5 and may help to revert tumor-infiltrating but exhausted NK cells into killers that produce perforin and IFN-γ. Decidual NK cells have previously been shown to possess two types of activity: they normally produce significant amounts of VEGF-A but stimulation with IL-15 switches them to cytotoxic cells (36). We find that cytokines present in the tumor microenvironment, such as IL-10, IL-12, IL-18, IL-21 and IFN-β, decrease the activity of STAT5 (reflected by reduced phosphorylation of STAT5-Y694) while enhancing expression of VEGF-A. These results are consistent with the notion that cytokine-induced STAT5 regulation acts to convert NK cells from cytotoxic killers to tumor promoters.

The development of STAT5 inhibitors is currently at the preclinical stage. To the best of our knowledge, no specific STAT5 inhibitor has entered clinical trials. Nevertheless, several inhibitors of the upstream JAK kinases have been approved by the FDA, e.g. for the treatment of rheumatoid arthritis, and are currently being tested in a wide variety of clinical studies. In patients with advanced myelofibrosis, the JAK1/2/3 inhibitor Ruxolitinib is of clinical benefit. It reduces the tumor burden associated with a reduction in the levels of cytokines including VEGF-A, which is most likely produced by the tumor cells themselves (37). Previous work has shown that long-term Ruxolitinib treatment impairs the maturation and cytolytic functions of NK cells. MPN patients treated with the inhibitor suffer from recurrent infections (38). We now extend these findings by showing that Ruxolitinib significantly increases the amount of VEGF-A in NK cells. Ruxolitinib treatment of mice injected with *v-abl*$^{+}$ lymphoma cells caused a significantly

enhanced tumor burden that depends on NK cell-derived VEGF-A. This NK-cell mediated effect is presumably important in cases of minimal residual disease (MRD) controlled by NK cells or in other situations where limited tumor burden is controlled by the immune system, as described in the EEE model (39). Under these circumstances NK cells keep the tumor in check and there is a delicate balance between tumor and immune cells. The balance can be disrupted by the presence of factors that suppress STAT5, such as cytokines or JAK-STAT inhibitors.

We conclude that treatment with inhibitors of STAT5 or its upstream kinase not only hampers the cytotoxic function of NK cells but might also induce *Vegf-A* expression, thereby worsening the prognosis. NK cells have also been shown to inhibit angiogenesis by secreting IFN-γ (40). The reduced release of IFN-γ in STAT5-deficient NK cells may contribute to angiogenesis, although the molecular details remain to be elucidated. It is becoming clear that NK cells are not mere killing machines but complex players with tightly controlled effector responses. These need to be thoroughly investigated before we can predict with confidence the outcome of STAT5-directed therapy. In the meantime, it is important to monitor very closely the tumor development in patients undergoing clinical trials of JAK/STAT inhibitors, with complementary anti-VEGF therapy indicated if tumor growth is accelerated.

Methods

Mice

Mice were bred on C57BL/6 background and maintained at the University of Veterinary Medicine Vienna under pathogen-free conditions. Following mice were studied: *Vegf-A*$^{fl/fl}$, *Vegf-A*$^{\Delta/\Delta}$*Ncr1*-iCre^{Tg}, *Stat5*$^{fl/fl}$*Mx1*-Cre (inducible Cre expression after type 1 interferon response, e.g. after Poly(I:C) injection), *Stat5*$^{fl/fl}$*Mx1*-Cre-*vav-bcl-2*, *Stat5*$^{\Delta/+}$*Ncr1*-iCre^{Tg}, *Stat5*$^{\Delta/\Delta}$*Ncr1*-iCre^{Tg},

Stat5$^{\Delta/\Delta}$*Ncr1*-iCre^{Tg}-*vav-bcl-2*, *Stat5*$^{fl/+}$, *Stat5*$^{fl/fl}$ and *vav-bcl-2* littermates (8,41–43). B10;B6-*Rag2*^{tm1Fwa} *Il2rg*^{tm1Wjl} mice (Taconic) were used for adoptive transfer experiments.

All experiments were carried out with age-matched 6-12 week old mice and were approved by the institutional animal care committee and review board conform to Austrian law (license 66.009/0019-II/10b/2010 14.1.10,68.205/0218-II/3b/2012 and BMWFW-68.205/0103-WF/V/3b/2015). *Stat5a*$^{-/-}$ and *Stat5b*$^{-/-}$ (44,45) were backcrossed with C57BL/6 once and then littermates were crossed for this study.

Cell culture

Splenic NK cells were isolated using the MACS positive selection kit (DX5, Miltenyi) and cultured with 5000U/ml rhIL-2 (Proleukin®, Roche). NK cell stimulations were performed in the presence of 5.000U/ml rhIL-2 ± 5ng/ml rmIL-12 (R&D), 50ng/ml rmIL-15 (PeproTech), 100U/ml rmIFN-β (Sigma), 5ng/ml rmIL-10 (R&D), 100ng/ml rmIL-21 (Immunotools), 50ng/ml rmIL-23 (R&D), 100ng/ml rmIL-18 (R&D), 50ng/ml rmIL-6 (R&D), 50ng/ml rmIL6Rα (R&D) or 10ng/ml Phorbol-12-myristat-13-acetat (PMA, Sigma) / 250ng/ml ionomycin (Sigma). For *in vitro* activation of Cre recombinase in NK cells expressing Mx-1Cre, IL-2 expanded NK cells were treated with 1000U/ml rmIFN-β (pbl Assay Science).

For inhibitor studies, splenic mouse or human peripheral blood NK cells were treated for 3 hours with 0.5/1μM Ruxolitinib (Chemietek) or 4 hours with a small-molecule STAT5-Inhibitor (46) and DMSO was used as vehicle control.

RMA and RMA-S cell lines were kindly provided by A.Cerewenka and authenticated by flow cytometry. *V-abl*$^{+}$ cell lines were generated in the laboratory of Prof.Veronika Sexl. All lines were tested for the presence of mycoplasm by PCR and surface marker expression by flow cytometry every 6 months (last authentication: November 2015).

Spheroid sprouting assays

Murine endothelial cells were suspended in 80% endothelial cell growth medium (RPMI containing 10% FCS mixed 1:1 with Endothelial Cell Growth Medium MV (PromoCell) and 20% methylcellulose (Sigma) and seeded as drops (800 cells/100µl) in nonadherent dishes. The dishes were incubated upside down as hanging drops for 24 hours. Under these conditions, all suspended cells contribute to the formation of a single spheroid per drop of defined size and cell number. Spheroids were harvested and seeded in a collagen matrix and supernatant of IL-2 expanded NK cells or 30ng/ml mVegf-A (PeproTech) was added. 2µg/ml LEAF™ purified anti-mouse VEGF-A Antibody (2G11-2A05, Biolegend) was added for the neutralization experiments. After 24-hours incubation, spheroids were scanned and photographed with an Olympus IX71 microscope using cellSens Dimension Software (Olympus). The sprout number and the cumulative length of the sprouts from each spheroid were calculated with ImageJ software.

Poly(I:C) treatment

Mice were treated three times by i.p. injection of 200µg Poly(I:C) (Invivogen) during 14 days. 7 days after the last injection mice were analysed. Activation of the Cre recombinase and deletion of *Stat5* results in a global *Stat5* deletion in *Stat5*$^{fl/fl}$*Mx1*-Cre and *Stat5*$^{fl/fl}$*Mx1*-Cre-*vav-bcl-2* including the entire hematopoietic compartment and is denoted as *Stat5*$^{\Delta/\Delta}$*Mx1*-Cre and *Stat5*$^{\Delta/\Delta}$*Mx1*-Cre-*vav-bcl-2*.

NK cell cytotoxicity

In vitro cytotoxicity assays were performed as previously published (25,47).

NK cell depletion

Mice were treated three times by i.p. injection of 100μg PK136 (anti-NK1.1.) antibody before s.c. injection of tumor cells and three times during the tumor progression. Successful deletion of $CD3^{-}NK1.1^{+}NKp46^{+}$ NK cells was checked in blood of treated animals by flow cytometry.

***In vivo* tumor challenge**

In the B16F10 melanoma model, mice were injected i.v. with $5x10^{4}$ B16F10 cells. After 23 days lungs were analysed. For survival assays, mice were sacrificed at first signs of dyspnea and health detractions.

In the *v-abl*, RMA and RMA-S tumor model, $5x10^{5}$-$5x10^{6}$ tumor cells were injected s.c. into the flanks of the mice and the health status was controlled daily. After 6-12 days mice were sacrificed and tumor weight was determined. Tumor diameters were measured with a caliper and the tumor volume in mm^{3} was calculated by the formula: Volume = $(width)^{2}$ x length/2.

In the A-MuLV model newborn mice were injected with 100 μL of replication- incompetent ecotropic retrovirus encoding for *v-abl* by s.c. injection as described previously (48). Mice were checked daily for disease onset.

Drug treatment of mice

Ruxolitinib (Chemietek) was dissolved to make a stock solution in DMSO and further diluted for oral gavage in PBS containing 0.5% methylcellulose (w/v) and 0.1% Tween 80. Mice were treated continuously once a day after tumor cell injection by oral gavage with 95mg/kg Ruxolitinib.

Antibodies and flow cytometry

The following antibodies (clones) were purchased from BD Biosciences: CD3ε(145-2C11), CD3(UCHT1), CD56(B159), CD16(3G8), CD11b(M1/70), CD27(LG.3A10), IFN-γ(XMG1.2) or purchased from eBioscience/Affymetrix: CD3ε(17A2, 145-2C11), CD49b(DX5), NK1.1(PK136), NKp46(29A1.4), Granzyme B(NGZB), T-bet(4B10), Eomes(Dan11mag) and Perforin (eBioOMAK-D). Granzyme A(3G8.5) was purchased from Santa-Cruz Biotechnology. Liver and lung were perfused and liver lymphocytes were obtained by a Percoll (GE Healthcare) gradient. Lung tissue was Collagenase/DNaseI (Sigma) digested prior to FACS staining. Bones were smashed with a mortar and filtered through a nylon mesh to obtain single cell suspension. Whole blood and splenocytes were depleted of erythrocytes and anti-CD16/CD32 (eBioscience) was added to all samples prior to staining. Intracellular stainings were performed with the Foxp3/Transcription factor staining buffer set (eBioscience) after application of a fixable viability dye (eBioscience). BrdU (Sigma) was injected i.p. 16 hours prior to analysis and incorporation was checked using an anti-BrdU antibody (BU20A, eBioscience) and DNase1 (Sigma) digestion according to eBioscience's protocol. Apoptosis stainings with IL-2 expanded NK cells were performed with Annexin V Apoptosis Detection Kit (eBioscience).

All samples were recorded on a FACS Canto II flow cytometer or sorted on a FACS Aria III (BD Biosciences) and analysed with BD FACS Diva software version 6.1.2 and 7.0.

Isolation of human peripheral blood NK cells

Blood of healthy donors was diluted 1:2 with 1xPBS and lymphocytes were isolated using LymphoPrep^{TM} (Axis Shield). $CD3^-CD56^+$,$CD3^-CD16^-CD56^{bright}$ and $CD3^-CD16^+CD56^+$ cells were sorted on a FACS AriaIII (BD) and RNA was isolated by RNeasy Micro Kit (Qiagen).

ChIP

MACS-purified and IL-2 cultured NK cells (10^7) were either left untreated or stimulated with IL-15 for 30 minutes followed by cross-linking using 1% formaldehyde for 10 min at 37 °C. The reaction was stopped by the addition of 0.5M glycine for 5 min. Cell nuclei were prepared and lysed in 1ml of lysis buffer on 4°C o/n. Chromatin was sheared by sonication yielding chromatin fragments between 200-500bp and diluted 2.5-fold in ChIP dilution buffer. IPs were performed at 4°C o/n with an anti-STAT5 antibody (C-17, sc-835, Santa Cruz Biotechnology). Chromatin was pre-cleared using 25µl salmon sperm DNA/protein A-agarose beads and incubated with the antibody o/n. Immune complexes were collected with 25µl beads for three hours and washed with RIPA buffer, high salt buffer, LiCl buffer and TE buffer. Samples were eluted twice in elution buffer (2% SDS, 10mM DTT and 100mM $NaHCO_3$). DNA cross-linking was reversed by heating at 65 °C o/n followed by proteinase K digestion. DNA was extracted with phenol-chloroform, precipitated in isopropanol and resuspended in TE Buffer. The predicted binding site was obtained using Ensemble for the sequence of the *Vegf-A* promoter and blasting for the potential STAT binding motif $TTC(N)_{2-4}GAA$. Obtained DNA fragments were analysed by qPCR using the following primer pairs: *Vegf-A*: Fw:5'-GCATGCATGTGTGTGTGTGT-3'and

Rev:5'- GGCAGGGACGTATGAGGATA-3', *Cish*: Fw:5'-CGCGCTGCTATTGGCCCTCCC -3'and Rev:5'-GTCTGGGGCCCTGAGCAGTG-3', *CD19*^{down}: Fw:5'-CCCTCTTCTCATTCGTTTTCCA-3'and Rev:5'-CCAGGAAAGAATTTGAGAAAAATCA -3'. N-fold enrichment was calculated relative to a negative region downstream of the CD19 gene (CD19^{down}).

Histology

Tumors were either paraformaldehyde-fixed and paraffin-embedded or OCT frozen. Sections (3μm) were stained with Hematoxylin/Eosin according to standard histological procedures. CD31 (cell signaling #9654S) stainings were performed as previously reported (49). The stainings were scanned and photographed with an Olympus IX71 or a Nikon Eclipse E1000 microscope using cellSens Dimension (Olympus) or NIS-elements (Nikon) software. Stainigs of CD31 and NKp46 (29A1.4, Biologend) and CD31 and F4/80 (CI:A3-1, ABD Serotec) were performed with frozen tumor sections as previously reported (50) and scanned with a LSM 5 Exciter (Zeiss) or a Nikon Eclipse E1000 microscope. Tumors were photographed and counted at random areas by three individual researches in a blinded manner.

Microarray

Data were extracted from ArrayExpress dataset E-GEOD-8059 and E-GEOD-50838 (Affymetrix Human Gene 1.1 ST Arrays). The heatmap was generated using *ClustVis* software (1). FDR, false discovery rate.

1. Metsalu T, Vilo J. ClustVis: a web tool for visualizing clustering of multivariate data using Principal Component Analysis and heatmap. Nucleic Acids Res. 2015 Jul 1;43(W1):W566-70. PubMed PMID: 25969447. Pubmed Central PMCID: 4489295.

Statistical analysis

Student's t-test, one-way ANOVA, Tukey's post hoc test and Mantel-Cox log-rank tests (survival curves) tests were performed using GraphPad Prism® Software version 5.04 and 6.02 (San Diego California USA). For multiple comparison of survival curves, Bonferroni- correction was applied. Statistical analysis is indicated for each experiment specifically (* $p < 0.05$; ** $p < 0.01$; *** $p < 0.001$).

Author Contributions

Contribution: D.G., E.M.P., E.S., E.G., M.P.-M., A.W.-S., P.K., G.H., Z.H. and C.S. performed the research, V.S., G.H., B.S., A.C. and P.T.G. provided reagents and analytic tools and analysed data; D.G., E.M.P., B.S., R.M., M.M., C.S and V.S. designed the research and wrote the manuscript.

Acknowledgements

We want to thank L. Edlinger, S. Fajmann, P. Jodl, H. Schachner and G. Asfour for all their help and G. Tebb for careful reading and revision of the manuscript and C. Moschner for helping with graphical illustrations of the sprouting assay We are grateful to the mouse facility. We were supported by the Austrian Science Fund FWF (grant SFB F28 and SFB F47) and the PhD program „Inflammation and Immunity“ FWF W1212.

References

1. Spits H, Artis D, Colonna M, Diefenbach A, Santo JP Di, Eberl G, et al. Innate lymphoid cells--a proposal for uniform nomenclature. Nat Rev Immunol. 2013;13:145–9.

2. Shi F-D, Ljunggren H-G, La Cava A, Van Kaer L. Organ-specific features of natural killer cells. Nat. Rev. Immunol. 2011. page 658–71.

3. Gotthardt D, Prchal-Murphy M, Seillet C, Glasner A, Mandelboim O, Carotta S, et al. NK cell development in bone marrow and liver: site matters. Genes Immun. 2014;15:584–7.

4. Hanna J, Goldman-Wohl D, Hamani Y, Avraham I, Greenfield C, Natanson-Yaron S, et al. Decidual NK cells regulate key developmental processes at the human fetal-maternal interface. Nat Med. 2006;12:1065–74.

5. Di Santo JP. Natural killer cell developmental pathways: a question of balance. Annu Rev Immunol. 2006;24:257–86.

6. Imada K, Leonard WJ. The Jak-STAT pathway. Mol Immunol. 2000;37:1–11.

7. Levy DE, Darnell JE. Stats: transcriptional control and biological impact. Nat Rev Mol Cell Biol. 2002;3:651–62.

8. Eckelhart E, Warsch W, Zebedin E, Simma O, Stoiber D, Kolbe T, et al. A novel Ncr1-Cre mouse reveals the essential role of STAT5 for NK cell survival and development. Blood. 2011;117:1565–73.

9. Hennighausen L, Robinson GW. Interpretation of cytokine signaling through the transcription factors STAT5A and STAT5B. Genes Dev. 2008;22:711–21.

10. Berger A, Sexl V, Valent P, Moriggl R. Inhibition of STAT5 : A therapeutic option in BCR-ABL1-driven leukemia. 2014;5:9564–76.

11. Bandapalli OR, Schuessele S, Kunz JB, Rausch T, Stütz AM, Tal N, et al. The activating STAT5B N642H mutation is a common abnormality in pediatric T-cell acute lymphoblastic leukemia and confers a higher risk of relapse. Haematologica. 2014;99:e188–92.

12. Küçük C, Jiang B, Hu X, Zhang W, Chan JKC, Xiao W, et al. Activating mutations of STAT5B and STAT3 in lymphomas derived from γδ-T or NK cells. Nat Commun. 2015;6:6025.

13. Debierre-Grockiego F. Anti-apoptotic role of STAT5 in haematopoietic cells and in the pathogenesis of malignancies. Apoptosis. 2004;9:717–28.

14. Aichberger KJ, Mayerhofer M, Krauth M-T, Skvara H, Florian S, Sonneck K, et al. Identification of mcl-1 as a BCR/ABL-dependent target in chronic myeloid leukemia (CML): evidence for cooperative antileukemic effects of imatinib and mcl-1 antisense oligonucleotides. Blood. 2005;105:3303–11.

15. Gesbert F, Griffin JD. Bcr/Abl activates transcription of the Bcl-X gene through STAT5. Blood. 2000;96:2269–76.

16. Warsch W, Grundschober E, Berger A, Gille L, Cerny-Reiterer S, Tigan A-S, et al. STAT5 triggers BCR-ABL1 mutation by mediating ROS production in chronic myeloid leukaemia. Oncotarget. 2012;3:1669–87.

17. Malin S, Mcmanus S, Cobaleda C, Novatchkova M, Delogu A, Bouillet P, et al. Role of STAT5 in controlling cell survival and immunoglobulin gene recombination during pro-B cell development. Nat Immunol. Nature Publishing Group; 2009;11:171–9.

18. Kim S, Iizuka K, Kang H-SPS, Dokun A, French AR, Greco S, et al. In vivo developmental stages in murine natural killer cell maturation. Nat Immunol. 2002;3:523–8.

19. Hayakawa Y, Huntington ND, Nutt SL, Smyth MJ. Functional subsets of mouse natural killer cells. Immunol Rev. 2006;214:47–55.

20. Sathe P, Delconte RB, Souza-Fonseca-Guimaraes F, Seillet C, Chopin M, Vandenberg CJ, et al. Innate immunodeficiency following genetic ablation of Mcl1 in natural killer cells. Nat Commun. 2014;5:4539.

21. Moriggl R, Topham DJ, Teglund S, Sexl V, McKay C, Wang D, et al. Stat5 is required for IL-2-induced cell cycle progression of peripheral T cells. Immunity. 1999/03/11 ed. 1999;10:249–59.

22. Hoelbl A, Schuster C, Kovacic B, Zhu B, Wickre M, Hoelzl MA, et al. Stat5 is indispensable for the maintenance of bcr/abl-positive leukaemia. EMBO Mol Med. 2010;2:98–110.

23. Smyth MJ, Cretney E, Kelly JM, Westwood JA, Street SE, Yagita H, et al. Activation of NK cell cytotoxicity. Mol Immunol. 2005;42:501–10.

24. Gotthardt D, Putz EM, Straka E, Kudweis P, Biaggio M, Poli V, et al. Loss of STAT3 in murine NK cells enhances NK cell-dependent tumor surveillance. Blood. 2014;124:2370–9.

25. Putz EM, Gotthardt D, Hoermann G, Csiszar A, Wirth S, Berger A, et al. CDK8-Mediated STAT1-S727 Phosphorylation Restrains NK Cell Cytotoxicity and Tumor Surveillance. Cell Rep. 2013;1–8.

26. Stoiber D, Kovacic B, Schuster C, Schellack C, Karaghiosoff M, Kreibich R, et al. TYK2 is a key regulator of the surveillance of B lymphoid tumors. J Clin Invest. 2004/12/04 ed. 2004;114:1650–8.

27. Wallin RPA, Screpanti V, Michaëlsson J, Grandien A, Ljunggren HG. Regulation of perforin-independent NK cell-mediated cytotoxicity. Eur J Immunol. 2003;33:2727–35.

28. Podar K, Anderson KC. The pathophysiologic role of VEGF in hematologic malignancies: therapeutic implications. Blood. 2005;105:1383–95.

29. Coffelt SB, Hughes R, Lewis CE. Tumor-associated macrophages: effectors of angiogenesis and tumor progression. Biochim Biophys Acta. 2009;1796:11–8.

30. Riabov V, Gudima A, Wang N, Mickley A, Orekhov A, Kzhyshkowska J. Role of tumor associated macrophages in tumor angiogenesis and lymphangiogenesis. Front Physiol. 2014;5 MAR:1–13.

31. Hennighausen L, Robinson GW. Interpretation of cytokine signaling through the transcription factors STAT5A and STAT5B. Genes Dev. 2008. page 711–21.

32. Zhang J, Scordi I, Smyth MJ, Lichtenheld MG. Interleukin 2 receptor signaling regulates the perforin gene through signal transducer and activator of transcription (Stat)5 activation of two enhancers. J Exp Med. 1999;190:1297–308.

33. Bruno A, Focaccetti C, Pagani A, Imperatori AS, Spagnoletti M, Rotolo N, et al. The proangiogenic phenotype of natural killer cells in patients with non-small cell lung cancer. Neoplasia. 2013;15:133–42.

34. Levi I, Amsalem H, Nissan A, Darash-Yahana M, Peretz T, Mandelboim O, et al. Characterization of tumor infiltrating natural killer cell subset. Oncotarget. 2015;6:13835–43.

35. Bruno A, Ferlazzo G, Albini A, Noonan DM. A think tank of TINK/TANKs: tumor-infiltrating/tumor-associated natural killer cells in tumor progression and angiogenesis. J Natl Cancer Inst. 2014;106:dju200.

36. Cerdeira AS, Rajakumar A, Royle CM, Lo A, Husain Z, Thadhani RI, et al. Conversion of peripheral blood NK cells to a decidual NK-like phenotype by a cocktail of defined factors. J Immunol. 2013;190:3939–48.

37. Verstovsek S, Kantarjian H, Mesa R a, Pardanani AD, Cortes-Franco J, Thomas D a, et al. Safety and efficacy of INCB018424, a JAK1 and JAK2 inhibitor, in myelofibrosis. N Engl J Med. 2010;363:1117–27.

38. Schönberg K, Rudolph J, Vonnahme M, Parampalli S, Cornez I, Hejazi M, et al. JAK inhibition impairs NK cell function. Cancer Res. 2015;

39. Mittal D, Gubin MM, Schreiber RD, Smyth MJ. New insights into cancer immunoediting and its three component phases--elimination, equilibrium and escape. Curr Opin Immunol. 2014;27:16–25.

40. Yao L, Sgadari C, Furuke K, Bloom ET, Teruya-Feldstein J, Tosato G. Contribution of natural killer cells to inhibition of angiogenesis by interleukin-12. Blood. 1999;93:1612–21.

41. Gerber H, Hillan K, Ryan A, Kowalski J. VEGF is required for growth and survival in neonatal mice. Apoptosis. 1999;1159:1149–59.

42. Kuhn R, Schwenk F, Aguet M, Rajewsky K. Inducible gene targeting in mice. Science (80-.). 1995. page 1427–9.

43. Ogilvy S, Metcalf D, Print CG, Bath ML, Harris AW, Adams JM. Constitutive Bcl-2 expression throughout the hematopoietic compartment affects multiple lineages and enhances progenitor cell survival. Proc Natl Acad Sci U S A. 1999;96:14943–8.

44. Liu X, Robinson GW, Wagner KU, Garrett L, Wynshaw-Boris A, Hennighausen L. Stat5a is mandatory for adult mammary gland development and lactogenesis. Genes Dev. 1997;11:179–86.

45. Udy GB, Towers RP, Snell RG, Wilkins RJ, Park SH, Ram P a, et al. Requirement of STAT5b for sexual dimorphism of body growth rates and liver gene expression. Proc Natl Acad Sci U S A. 1997;94:7239–44.

46. Cumaraswamy A a, Lewis AM, Geletu M, Todic A, Diaz DB, Cheng XR, et al. Nanomolar-Potency Small Molecule Inhibitor of STAT5 Protein. ACS Med Chem Lett. 2014;5:1202–6.

47. Mizutani T, Neugebauer N, Putz EM, Moritz N, Simma O, Zebedin-Brandl E, et al. Conditional IFNAR1 ablation reveals distinct requirements of Type I IFN signaling for NK cell maturation and tumor surveillance. Oncoimmunology. 2012;1:1027–37.

48. Sexl V, Piekorz R, Moriggl R, Rohrer J, Brown MP, Bunting KD, et al. Stat5a/b contribute to interleukin 7-induced B-cell precursor expansion, but abl- and bcr/abl-induced transformation are independent of Stat5. Blood. 2000;96:2277–83.

49. Putz EM, Hoelzl MA, Baeck J, Bago-Horvath Z, Schuster C, Reichholf B, et al. Loss of STAT3 in Lymphoma Relaxes NK Cell-Mediated Tumor Surveillance. Cancers (Basel). Multidisciplinary Digital Publishing Institute; 2014;6:193–210.

50. Pathria P, Gotthardt D, Prchal-Murphy M, Putz E-M, Holcmann M, Schlederer M, et al. Myeloid STAT3 promotes formation of colitis-associated colorectal cancer in mice. Oncoimmunology. 2015;4:e998529.

Figure Legends

Figure 1: Overexpression of *Bcl-2* suffices to rescue NK cells in the absence of STAT5 and reveals a role of STAT5 in NK cell maturation. (A) Splenocytes of *Stat5*$^{fl/+}$ and *Stat5*$^{\Delta/+}$*Ncr1*-iCre^{Tg} mice were stained for CD3 and NKp46 and analysed by flow cytometry for the percentage of CD3$^-$NKp46$^+$ NK cells gated on lymphocytes. Bar graphs depict mean±SEM (n=13 per genotype). Unpaired t-test was used for statistical analysis. (B) Total NK cell number of splenic CD3$^-$NKp46$^+$ NK cells of *Stat5*$^{fl/fl}$, *Stat5*$^{\Delta/\Delta}$*Ncr1*-iCre^{Tg}, *vav-bcl-2* and *Stat5*$^{\Delta/\Delta}$*Ncr1*-iCre^{Tg}-*vav-bcl-2* mice. Splenocytes were analysed by flow cytometry and total cell numbers were calculated. One representative out of 5 independent experiments with n≥5 per genotype is shown. Bar graphs depict mean±SEM, Tukey's post-hoc test was applied for statistical analysis. (C) RNA was isolated of MACS-purified and IL-2 cultured *Stat5*$^{fl/fl}$, *Stat5*$^{\Delta/\Delta}$*Ncr1*-iCre^{Tg}-*vav-bcl-2* and *vav-bcl-2* NK cells and transcribed into cDNA used for qPCR expression analysis of *Stat5a* and *Stat5b*. Data represent means±SEM of two independent experiments. Expression levels were calculated relative to the housekeeping gene *Rplp0* and all values were normalized to *Stat5*$^{fl/fl}$ NK cells. Tukey's post-hoc test was applied for statistical analysis. (D+E) For the analysis of NK cell maturation stages, *Stat5*$^{fl/fl}$, *Stat5*$^{\Delta/+}$*Ncr1*-iCre^{Tg}, *Stat5*$^{\Delta/\Delta}$*Ncr1*-iCre^{Tg}-*vav-bcl-2*, *Stat5*$^{\Delta/+}$*Mx1*-Cre, *Stat5*$^{\Delta/\Delta}$*Mx1*-Cre-*vav-bcl-2* and *vav-bcl-2* splenic CD3$^-$NKp46$^+$ NK cells were analysed for CD27 and CD11b expression by flow cytometry. Data are representative for at least two independent experiments with n≥7 per genotype (n=3 for *Stat5*$^{\Delta/+}$*Mx1*-Cre). Numbers represent mean±SEM. Tukey's post-hoc test was applied for statistical analysis of each maturation stage. *Stat5*$^{\Delta/+}$*Mx1*-Cre and *Stat5*$^{\Delta/\Delta}$*Mx1*-Cre-*vav-bcl-2* and respective controls were Poly(I:C) treated (resulting in an type I interferon response) to induce Cre activation.

Figure 2: STAT5-deficient NK cells possess an aberrant transcription factor expression, hampered proliferation and an impaired lytic machinery. (A) RNA was isolated of MACS-purified and IL-2 cultured *Stat5*$^{fl/fl}$, *Stat5*$^{\Delta/+}$*Ncr1*-iCre^{Tg}, *Stat5*$^{\Delta/\Delta}$*Ncr1*-iCre^{Tg}-*vav-bcl-2* and *vav-bcl-2* NK cells and transcribed into cDNA for qPCR expression analysis of *Id2, Tbx21* and *Eomes.* Data represent means±SEM of two independent experiments. Expression levels were calculated relative to the housekeeping gene *Rplp0* and all values were normalized to *Stat5*$^{fl/fl}$ NK cells. Tukey's post-hoc test was applied for statistical analysis. (B) MACS-purified *Stat5*$^{fl/fl}$, *Stat5*$^{\Delta/\Delta}$*Ncr1*-iCre^{Tg}-*vav-bcl-2* and *vav-bcl-2* NK cells were IL-2 cultured and living cells were counted every day for growth curve analysis. One representative experiment out of three with similar outcome is shown. Tukey's post-hoc test was applied for statistical analysis of each time point. (C) BrdU was injected i.p. into mice of the respective genotypes. After 16 hours, splenic cells were isolated and stained for CD3$^-$NKp46$^+$, fixated, permeabilized, treated with DNase1, stained with anti-BrdU and analysed by flow cytometry. Data represent means±SEM (n≥4 per genotype) Tukey's post-hoc test was applied for statistical analysis. (D) RNA was isolated of MACS-purified and IL-2 cultured *Stat5*$^{fl/fl}$, *Stat5*$^{\Delta/\Delta}$*Ncr1*-iCre^{Tg}-*vav-bcl-2* and *vav-bcl-2* NK cells and transcribed into cDNA used for qPCR expression analysis of *Ccnd2 and Myc*. Data represent means±SEM of two independent experiments. Expression levels were calculated relative to the housekeeping gene *Rplp0* and all values were normalized to *Stat5*$^{fl/fl}$ NK cells. Tukey's post-hoc test was applied for statistical analysis. (E) RNA was isolated of MACS-purified and IL-2 cultured *Stat5*$^{fl/fl}$, *Stat5*$^{\Delta/\Delta}$*Ncr1*-iCre^{Tg}-*vav-bcl-2* and *vav-bcl-2* NK cells and transcribed into cDNA for qPCR expression analysis of *Prf1, Grzma, Grzmb* and *Ifng.* Data represent means±SEM of two independent experiments. Expression levels were calculated relative to the housekeeping gene *Rplp0* and all values were normalized to *Stat5*$^{fl/fl}$ NK cells. Tukey's post-hoc test was applied for statistical analysis. (F) *In vitro* cytotoxicity assay of IL-2-expanded primary

NK cells and RMA-S (left panel) or YAC-1 (right panel) target cell lines. The effector:target (E:T) cell ratios ranged from 1:1 to 10:1 and after 4 hours incubation on 37°C the lysis of the targets cells was analysed by flow cytometry. Symbols represent means and error bars indicate SEM of triplicates. Tukey's post-hoc test was applied for statistical analysis of each E:T ratio. Data are representative of at least two independent experiments with similar outcome.

Figure 3: STAT5-deficient NK cells show reduced cytolytic capacity. (A+B) $5x10^4$ B16F10 melanoma cells were injected i.v. into *Stat5*$^{fl/fl}$, *Stat5*$^{\Delta/\Delta}$*Ncr1*-iCre^{Tg}, *Stat5*$^{\Delta/\Delta}$*Ncr1*-iCre^{Tg}-*vav-bcl-2* mice and *vav-bcl-2* (n≥6 per genotype). (A) Mice were sacrificed at first signs of paralysis and health detractions. For statistical analysis a Bonferroni-corrected log rank test was applied. (B) The number of tumor nodules in the lung was assessed after 23 days. Tukey's post-hoc test was applied for statistical analysis. (C+D) 10^6 *v-abl*$^+$ leukemic cells were injected s.c. in the flanks of *Stat5*$^{fl/fl}$, *Stat5*$^{\Delta/\Delta}$*Ncr1*-iCre^{Tg}, *vav-bcl-2* and *Stat5*$^{\Delta/\Delta}$*Ncr1*-iCre^{Tg}-*vav-bcl-2* mice. Data represent means±SEM of three independent experiments (n≥18 per genotype). After 6 days the tumor weight was determined and documented by (C) photographs representing one out of three independent experiments with similar outcome. (D) Statistics represent means±SEM of two independent experiments. Tukey's post-hoc test was applied for statistical analysis. (E) Tumor growth curve of *v-abl*$^+$ s.c. tumors in *Stat5*$^{fl/fl}$, *Stat5*$^{\Delta/\Delta}$*Ncr1*-iCre^{Tg}, *vav-bcl-2* and *Stat5*$^{\Delta/\Delta}$*Ncr1*-iCre^{Tg}-*vav-bcl-2* mice. Tukey's post-hoc test was applied for statistical analysis of each time point. (F) NK cells were depleted twice before and after s.c. injections of 10^6 *v-abl* cells. After 10 days the tumor weight of *Stat5*$^{fl/fl}$, *Stat5*$^{\Delta/\Delta}$*Ncr1*-iCre^{Tg}, *Stat5*$^{\Delta/\Delta}$*Ncr1*-iCre^{Tg}-*vav-bcl-2* and *vav-bcl-2* mice (n≥4 per genotype) was determined. There is no significant increase in the tumor burden of NK cell depleted *Stat5*$^{fl/fl}$ and *vav-bcl-2* mice as the experiment was terminated at an early time point. Tukey's post-hoc test was applied for statistical analysis.

Figure 4: *Stat5*$^{\Delta/\Delta}$*Ncr1*-iCre^{Tg}-*vav-bcl-2* NK cells have the potential to trigger tumor promotion and show increased production of VEGF-A. (A+B) 5x10^5 RMA cells were injected s.c. in the flanks of the mice (n≥12 per genotype). After 14 days the tumor weight was determined and documented by (A) photographs representing one out of two independent experiments with similar outcome. (B) Statistics represent means±SEM of two independent experiments. Tukey's post-hoc test was applied for statistical analysis. (C) NK cells were depleted twice before and after s.c. injections of 5x10^5 RMA cells. After 14 days the tumor weight of *Stat5*$^{fl/fl}$ and *Stat5*$^{\Delta/\Delta}$*Ncr1*-iCre^{Tg}-*vav-bcl-2* mice (n≥4 per genotype) was determined. Tukey's post-hoc test was applied for statistical analysis. (D) RNA was isolated of MACS-purified and IL-2 cultured *Stat5*$^{fl/fl}$, *Stat5*$^{\Delta/\Delta}$*Ncr1*-iCre^{Tg}-*vav-bcl-2* and *vav-bcl-2* NK cells and transcribed into cDNA for qPCR expression analysis of *Vegf-A*. Data represent means±SEM of two independent experiments. Expression levels were calculated relative to the housekeeping gene *Rplp0* and all values were normalized to *Stat5*$^{fl/fl}$ NK cells. Tukey's post-hoc test was applied for statistical analysis. (E+F) Spheroids of endothelial cells were embedded into a collagen matrix and IL-2 media (control), supernantant of IL-2 cultured *Stat5*$^{fl/fl}$, *Stat5*$^{\Delta/\Delta}$*Ncr1*-iCre^{Tg}-*vav-bcl-2* and *vav-bcl-2* NK cells or mVEGF-A (positive control) were added and sprouting was documented after 24 hours. (E) Representative pictures of one experiment out of two (with similar outcome) are depicted. (F) Average sprout number and cumulative sprouting length was quantified by ImageJ software. Tukey's post-hoc test was applied for statistical analysis.

Figure 5: NK cell-derived VEGF-A promotes tumorigenesis. (A+B) 10^6 *v-abl*$^+$ cells were injected s.c. in the flanks of the *Vegf-A*$^{fl/fl}$ and *Vegf-A*$^{\Delta/\Delta}$*Ncr1*-iCre^{Tg} mice. After 12 days tumor weight was determined and documented by (A) photographs representing one out of three

independent experiments with similar outcome. (B) Statistics represent means±SEM of three independent experiments (n≥27 per genotype). Unpaired t-test was applied for statistical analysis. (C) Tumor growth curve of *v-abl*$^{+}$ s.c. tumors in *Vegf-A*$^{fl/fl}$ and *Vegf-A*$^{\Delta/\Delta}$*Ncr1*-iCre^{Tg} mice. Unpaired t-terst was applied for statistical analysis of the indicated time points. (D) CD31 staining of *v-abl*$^{+}$ tumors (random representative areas) derived from *Vegf-A*$^{fl/fl}$ and *Vegf-A*$^{\Delta/\Delta}$*Ncr1*-iCre^{Tg} mice. Number of CD31^{+} cells per specific field of different tumor sections were counted by two independent researchers in a blinded manner. Unpaired t-test was applied for statistical analysis. (E) Newborn *Vegf-A*$^{fl/fl}$ (n=8) and *Vegf-A*$^{\Delta/\Delta}$*Ncr1*-iCre^{Tg} (n=10) mice were injected s.c. with a replication-incompetent ecotropic retrovirus encoding for *v-abl*. Mice were sacrificed at first signs of paralysis and health detractions. Mantel-Cox log-rank tests was applied for statistical analysis. (F) CD31 (green) and NKp46 (red) co-stainings of *v-abl*$^{+}$ tumors (random representative areas) derived from *Vegf-A*$^{fl/fl}$ and *Vegf-A*$^{\Delta/\Delta}$*Ncr1*-iCre^{Tg} mice. Number of CD31^{+} and NKp46^{+} cells of different tumor sections were counted by two independent researchers in a blinded manner. Number of CD31^{+} cells per specific field was significantly reduced in tumors derived from *Vegf-A*$^{\Delta/\Delta}$*Ncr1*-iCre^{Tg} mice, while the number of infiltrating NK cells was unchanged. NK cell/CD31^{+} cell ratio is shown. Unpaired t-test was applied for statistical analysis.

Figure 6: STAT5B suppresses VEGF-A production by directly binding to its promoter.

(A) *Ex vivo*-derived MACS-purified and sorted NK cells were stimulated for 2 hours with IL-2 or IL-2+ IL-15 (2 or 4 hours). RNA was isolated and transcribed into cDNA used for qPCR analysis of *Vegf-A* mRNA levels. Data represent means±SEM of two independent experiments. Expression levels were calculated relative to the housekeeping gene *Rplp0* and all values were normalized to stimulation with IL-2 (2 hours) highlighting the relative decrease. Tukey's post-hoc test was applied for statistical analysis. (B) Primary IL-2 cultured NK cells were stimulated

for 30 minutes with IL-2 or IL-2+IL-15. The reaction was stopped by addition of formaldehyde. ChIP was performed using an anti-STAT5 antibody and n-fold-enrichment of *Vegf-A* or *Cish* (positive control) was calculated relative to the expression of a negative region ("CD19 down"). Statistics represent means±SEM of three independent experiments and tukey's post-hoc test was applied for statistical analysis. (C) MACS-purified and IL-2 expanded C57BL/6 WT NK cells were stimulated with the respective cytokines for 60 and 200 minutes. Stimulated NK cells were harvested and protein lysates were used for western blot to detect pStat5-Y694. ß-Actin was used as loading control. (D) *Stat5 WT (+/+)*, *Stat5a-/-* and *Stat5b-/-* NK cells were MACS-purified and IL-2 expanded for 5 days. RNA was isolated and transcribed into cDNA used for qPCR analysis of *Vegf-A* mRNA levels. Data represent means±SEM of two independent experiments. Expression levels were calculated relative to the housekeeping gene *Rplp0* and all values were normalized to *Stat5 WT (+/+)* NK cells. Tukey's post-hoc test was applied for statistical analysis. (E) Lymphocytes of healthy human blood donors (n=8) were enriched and $CD16^{-}CD56^{bright}$ and $CD16^{+}CD56^{+}$ NK cells were sorted. RNA was isolated and transcribed into into cDNA for qPCR analysis of human *STAT5A*, *STAT5B*, *VEGF-A* and *BCL2* mRNA levels. Expression levels were calculated relative to the housekeeping gene *Rplp0* and all values were normalized to $CD16^{+}CD56^{+}$cells. Unpaired t-test was used for statistical analysis showing that $CD16^{+}CD56^{+}$cells have higher expression levels of *STAT5A* and *STAT5B* but lower expression of *VEGF-A* compared to $CD16^{-}CD56^{bright}$ cells. (F) Scatter plot showing expression microarray data of resting and IL-2 stimulated human NK cells. Expression values of STAT5A, STAT5B, VEGF-A, EOMES, CCND2 and CISH are highlighted. Microarray data were obtained from ArrayExpress database (E-GEOD-8059).

Figure 7: The upstream kinase inhibitor increases NK cell-derived *Vegf-A* expression and enhances tumor promotion *in vivo.*

(A) IL-2 expanded murine NK cells were treated with 0.5µM Ruxolitinib or a vehicle control (DMSO) for 3 hours and stimulated in the last hour additional with IL-2. NK cell-derived *Vegf-A* mRNA production was analysed by qPCR and calculated relative to the house keeping gene *Rplp0*. Data represent means±SEM of two independent experiments. Expression levels were normalized to the vehicle control. Unpaired t-test was applied for statistical analysis (B) Human blood NK cells were sorted ($CD3^-CD56^+$, n=4) and treated with 0.5µM, 1µM Ruxolitinib or a vehicle control (DMSO) for 3 hours and stimulated in the last hour with 500U IL-2. pSTAT5-Y694 as well as STAT5A/B was detected by western blotting. (C) Human blood NK cells were sorted ($CD3^-CD56^+$, n=4) and treated with 0.5µM Ruxolitinib or a vehicle control (DMSO) for 3 hours and stimulated in the last hour with 500U IL-2. NK-cell derived *VEGF-A* mRNA production was analysed by qPCR and calculated relative to the house keeping gene *RPLP0*. Expression levels were normalized to the vehicle control. Unpaired t-test was applied for statistical analysis. (D) 10^6 *v-abl*$^+$ cells were injected s.c. in the flanks of the *Vegf-A*$^{fl/fl}$ and *Vegf-A*$^{\Delta/\Delta}$*Ncr1*-iCre^{Tg} mice. After tumor cell injection mice were treated once a day with Ruxolitinib or a vehicle control by oral gavage. After 8 days tumor weight was determined and documented by photographs (left). Statistics (right) represent means±SEM (n≥8 per genotype). Tukey's post-hoc test was applied for statistical analysis. (E) Tumor growth curve of *v-abl*$^+$ s.c. tumors injected into *Vegf-A*$^{fl/fl}$ and *Vegf-A*$^{\Delta/\Delta}$*Ncr1*-iCre^{Tg} mice treated with Ruxolitinib or a vehicle control. Tukey's post-hoc test was applied for statistical analysis of each individual time point.

Figure 1

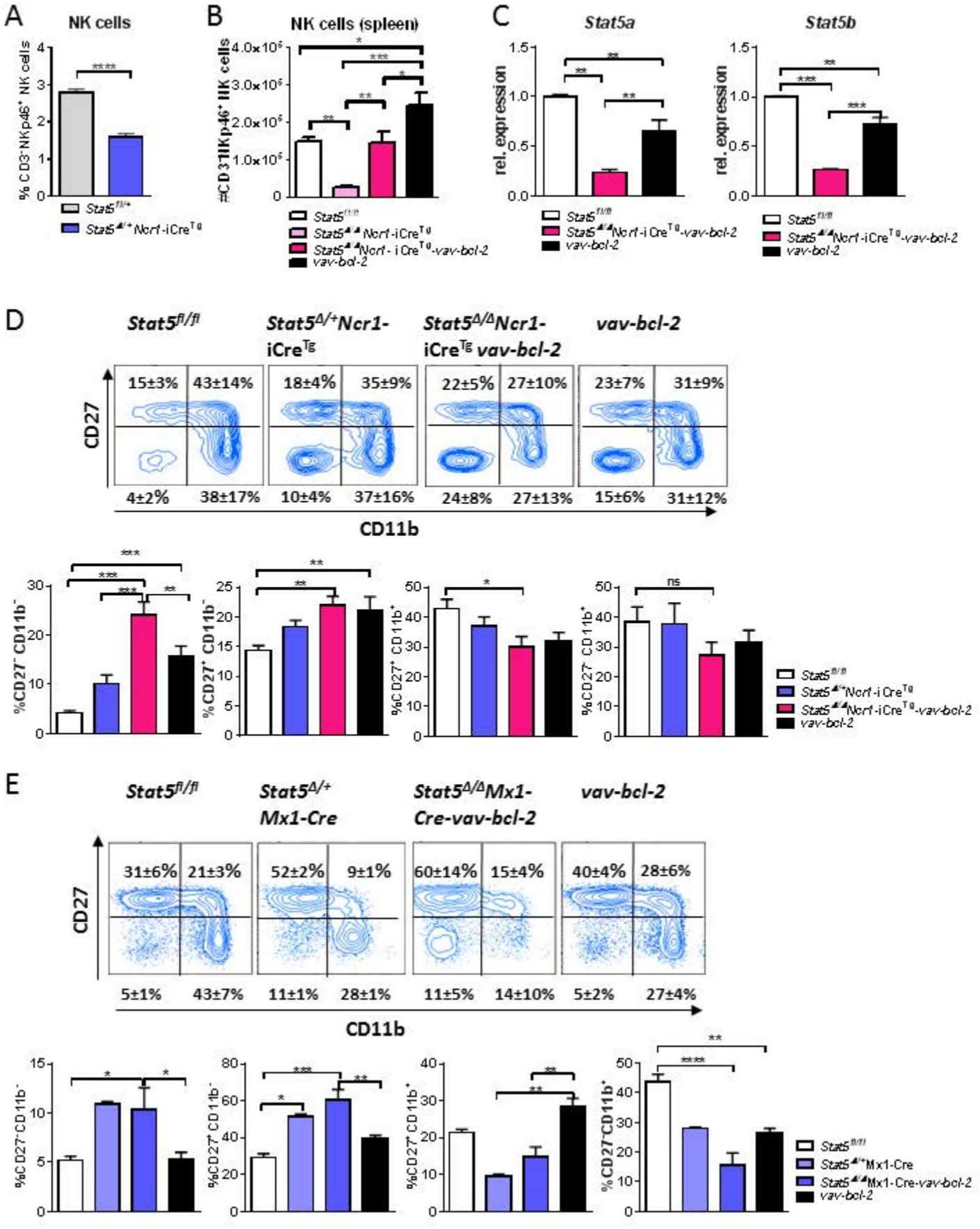
A
NK cells
% CD3⁻NKp46⁺ NK cells
Stat5fl/+
Stat5Δ/+Ncr1-iCreTg
B
NK cells (spleen)
#CD3⁻NKp46⁺ NK cells
Stat5fl/fl
Stat5Δ/ΔNcr1-iCreTg
Stat5Δ/ΔNcr1-iCreTg-vav-bcl-2
vav-bcl-2
C
Stat5a
Stat5b
rel. expression
Stat5fl/fl
Stat5Δ/ΔNcr1-iCreTg-vav-bcl-2
vav-bcl-2
D
Stat5fl/fl
Stat5Δ/+Ncr1-iCreTg
Stat5Δ/ΔNcr1-iCreTg vav-bcl-2
vav-bcl-2
CD27
CD11b
15±3%
43±14%
18±4%
35±9%
22±5%
27±10%
23±7%
31±9%
4±2%
38±17%
10±4%
37±16%
24±8%
27±13%
15±6%
31±12%
%CD27⁻CD11b⁻
%CD27⁺CD11b⁻
%CD27⁺CD11b⁺
%CD27⁻CD11b⁺
ns
Stat5fl/fl
Stat5Δ/+Ncr1-iCreTg
Stat5Δ/ΔNcr1-iCreTg-vav-bcl-2
vav-bcl-2
E
Stat5fl/fl
Stat5Δ/+ Mx1-Cre
Stat5Δ/ΔMx1-Cre-vav-bcl-2
vav-bcl-2
CD27
CD11b
31±6%
21±3%
52±2%
9±1%
60±14%
15±4%
40±4%
28±6%
5±1%
43±7%
11±1%
28±1%
11±5%
14±10%
5±2%
27±4%
%CD27⁻CD11b⁻
%CD27⁺CD11b⁻
%CD27⁺CD11b⁺
%CD27⁻CD11b⁺
Stat5fl/fl
Stat5Δ/+Mx1-Cre
Stat5Δ/ΔMx1-Cre-vav-bcl-2
vav-bcl-2

Figure 2

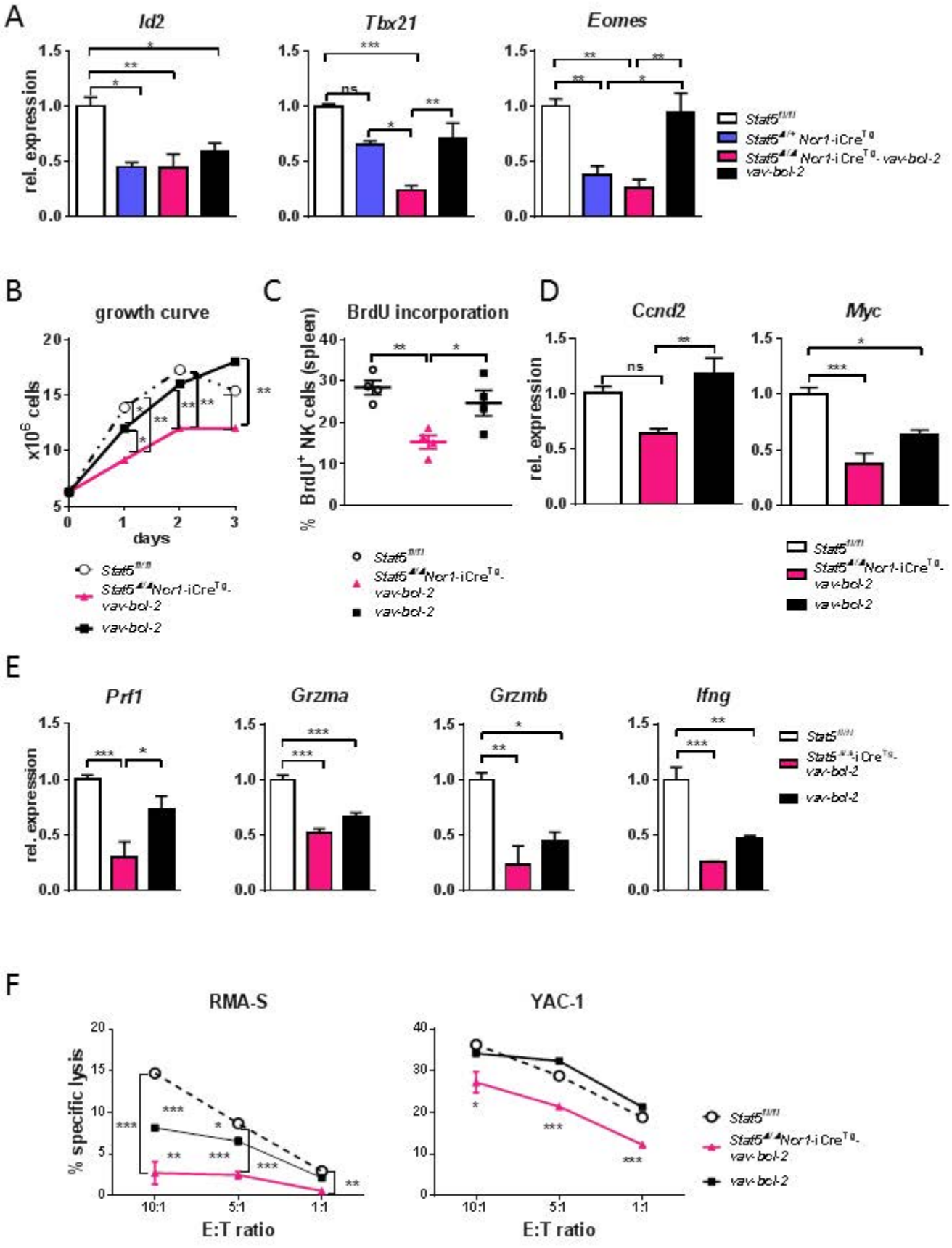
A
Id2
Tbx21
Eomes
rel. expression
Stat5fl/fl
Stat5Δ/+ Ncr1-iCreTg
Stat5Δ/Δ Ncr1-iCreTg- vav-bcl-2
vav-bcl-2
B
growth curve
x10^6 cells
days
Stat5fl/fl
Stat5Δ/ΔNcr1-iCreTg- vav-bcl-2
vav-bcl-2
C
BrdU incorporation
% BrdU+ NK cells (spleen)
Stat5fl/fl
Stat5Δ/ΔNcr1-iCreTg- vav-bcl-2
vav-bcl-2
D
Ccnd2
Myc
rel. expression
Stat5fl/fl
Stat5Δ/ΔNcr1-iCreTg- vav-bcl-2
vav-bcl-2
E
Prf1
Grzma
Grzmb
Ifng
rel. expression
Stat5fl/fl
Stat5Δ/ΔiCreTg- vav-bcl-2
vav-bcl-2
F
RMA-S
YAC-1
% specific lysis
E:T ratio
10:1
5:1
1:1
Stat5fl/fl
Stat5Δ/ΔNcr1-iCreTg- vav-bcl-2
vav-bcl-2

Figure 3

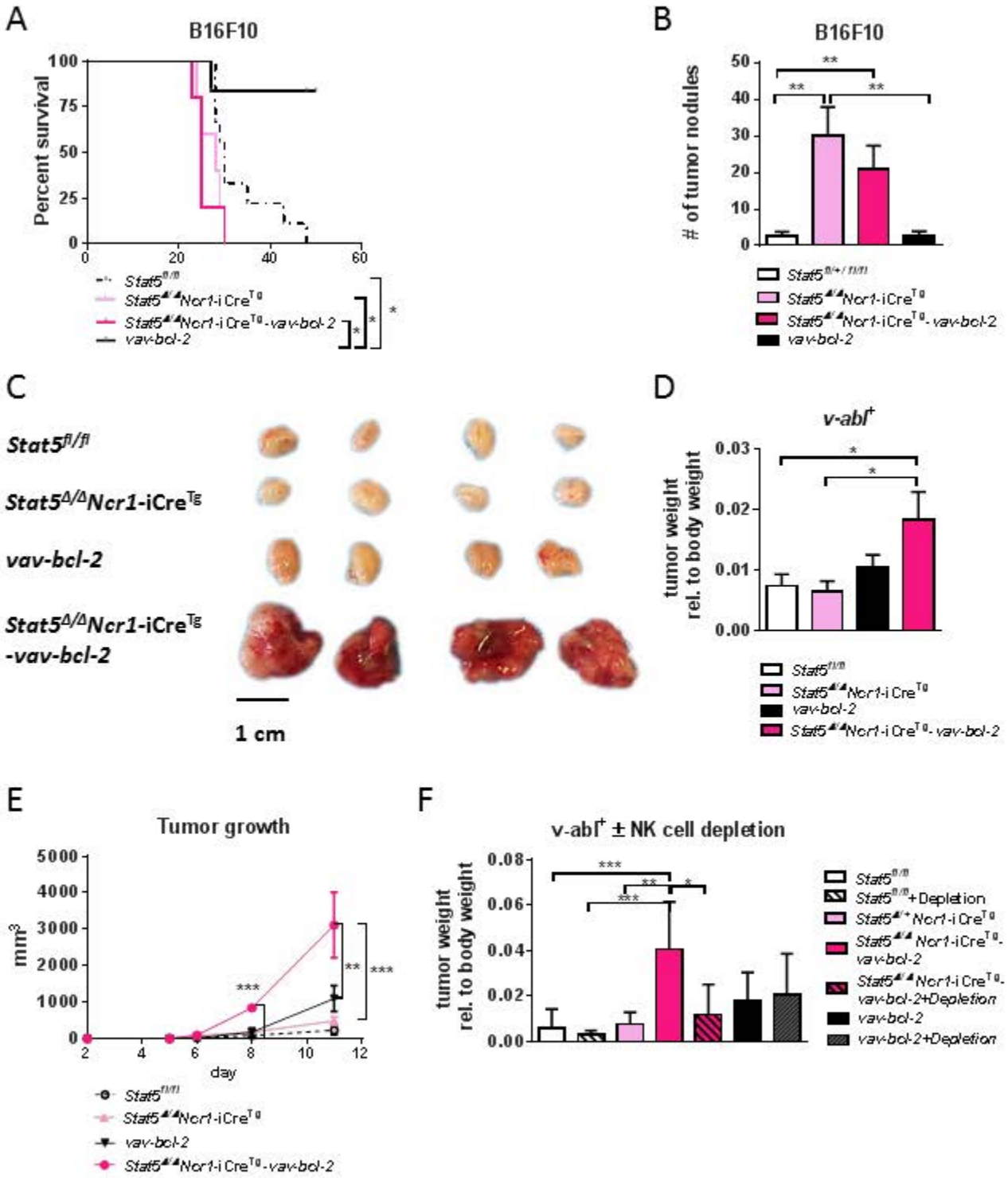
A
B16F10
Percent survival
100
75
50
25
0
0
20
40
60
Stat5fl/fl
Stat5Δ/ΔNcr1-iCreTg
Stat5Δ/ΔNcr1-iCreTg-vav-bcl-2
vav-bcl-2
B
B16F10
# of tumor nodules
50
40
30
20
10
0
Stat5fl/+/fl/fl
Stat5Δ/ΔNcr1-iCreTg
Stat5Δ/ΔNcr1-iCreTg-vav-bcl-2
vav-bcl-2
C
Stat5fl/fl
Stat5Δ/ΔNcr1-iCreTg
vav-bcl-2
Stat5Δ/ΔNcr1-iCreTg
-vav-bcl-2
1 cm
D
v-ablt
tumor weight
rel. to body weight
0.03
0.02
0.01
0.00
Stat5fl/fl
Stat5Δ/ΔNcr1-iCreTg
vav-bcl-2
Stat5Δ/ΔNcr1-iCreTg-vav-bcl-2
E
Tumor growth
mm3
5000
4000
3000
2000
1000
0
2
4
6
8
10
12
day
Stat5fl/fl
Stat5Δ/ΔNcr1-iCreTg
vav-bcl-2
Stat5Δ/ΔNcr1-iCreTg-vav-bcl-2
F
v-ablt ± NK cell depletion
tumor weight
rel. to body weight
0.08
0.06
0.04
0.02
0.00
Stat5fl/fl
Stat5fl/fl+Depletion
Stat5Δ/+Ncr1-iCreTg
Stat5Δ/ΔNcr1-iCreTg-vav-bcl-2
Stat5Δ/ΔNcr1-iCreTg-vav-bcl-2+Depletion
vav-bcl-2
vav-bcl-2+Depletion

Figure 4

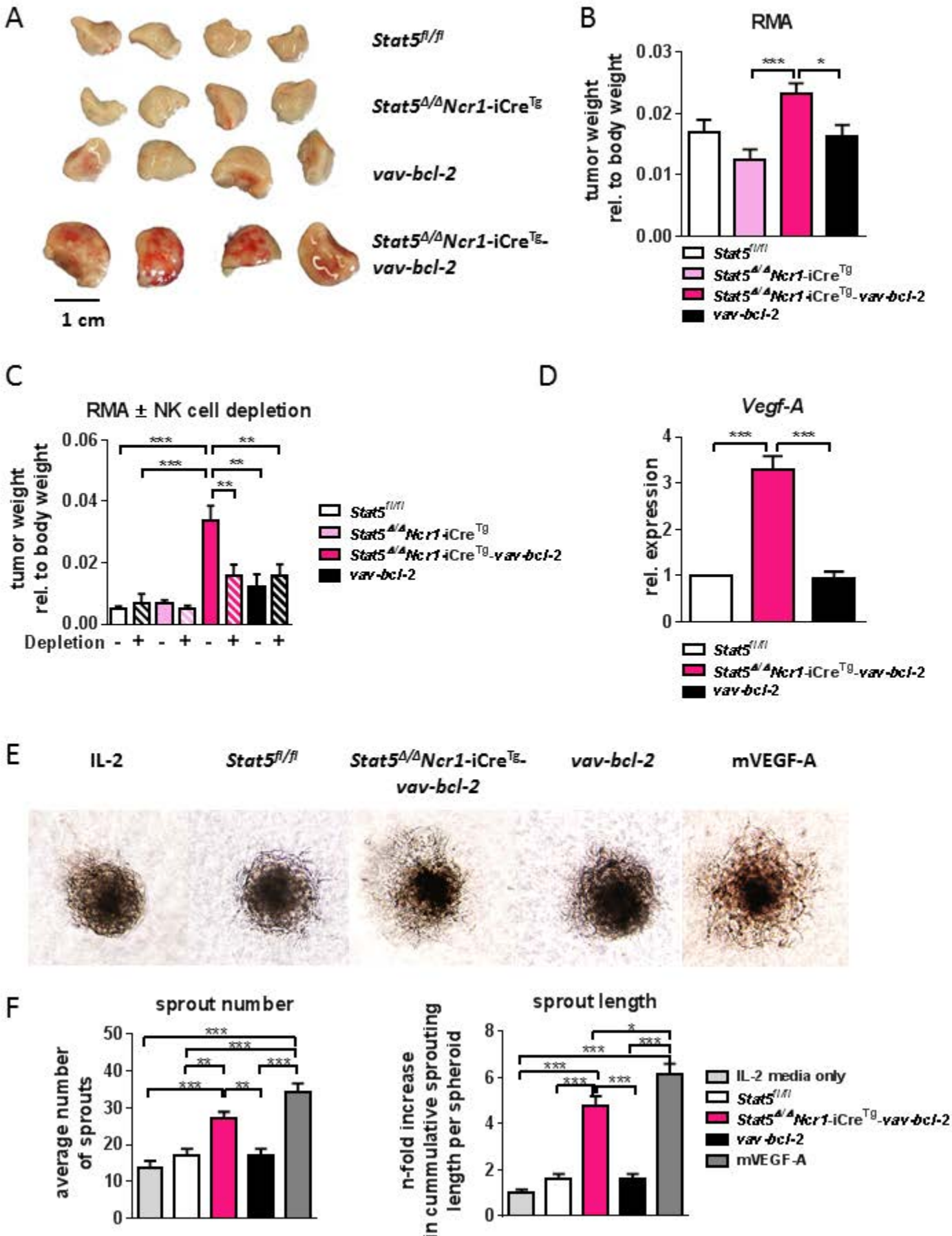
A
Stat5fl/fl
Stat5Δ/ΔNcr1-iCreTg
vav-bcl-2
Stat5Δ/ΔNcr1-iCreTg-vav-bcl-2
1 cm
B
RMA
tumor weight rel. to body weight
0.03
0.02
0.01
0.00
***
*
Stat5fl/fl
Stat5Δ/ΔNcr1-iCreTg
Stat5Δ/ΔNcr1-iCreTg-vav-bcl-2
vav-bcl-2
C
RMA ± NK cell depletion
tumor weight rel. to body weight
0.06
0.04
0.02
0.00
***
**
Depletion - + - + - + - +
Stat5fl/fl
Stat5Δ/ΔNcr1-iCreTg
Stat5Δ/ΔNcr1-iCreTg-vav-bcl-2
vav-bcl-2
D
Vegf-A
rel. expression
4
3
2
1
0
***
Stat5fl/fl
Stat5Δ/ΔNcr1-iCreTg-vav-bcl-2
vav-bcl-2
E
IL-2
Stat5fl/fl
Stat5Δ/ΔNcr1-iCreTg-vav-bcl-2
vav-bcl-2
mVEGF-A
F
sprout number
average number of sprouts
50
40
30
20
10
0
***
**
sprout length
n-fold increase in cummulative sprouting length per spheroid
8
6
4
2
0
*
IL-2 media only
Stat5fl/fl
Stat5Δ/ΔNcr1-iCreTg-vav-bcl-2
vav-bcl-2
mVEGF-A

Figure 5

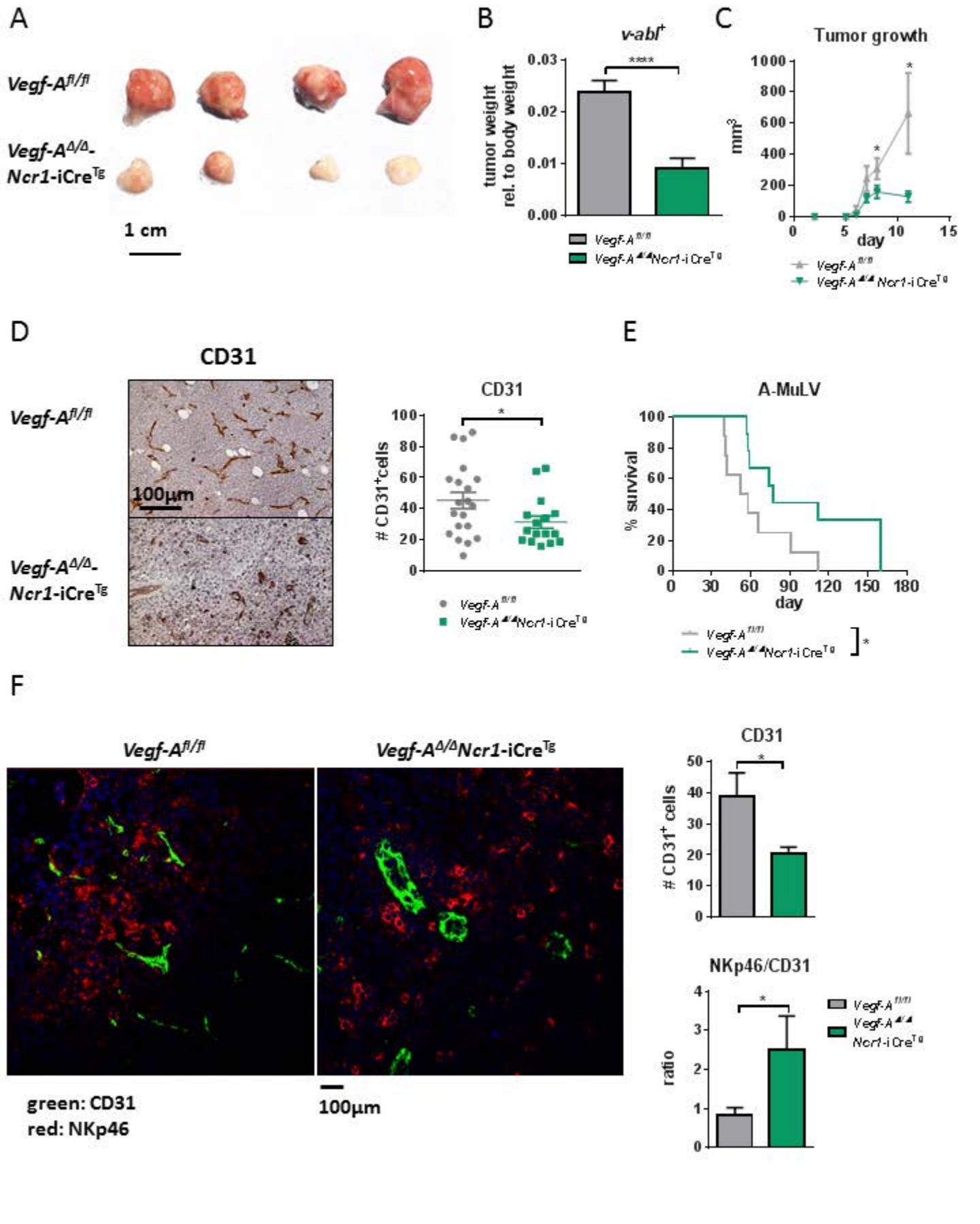
A
Vegf-A fl/fl
Vegf-A Δ/Δ-Ncr1-iCre Tg
1 cm
B
v-abl+
tumor weight rel. to body weight
0.03
0.02
0.01
0.00
****
Vegf-A fl/fl
Vegf-A Δ/Δ Ncr1-iCre Tg
C
Tumor growth
mm3
1000
800
600
400
200
0
0
5
10
15
day
*
Vegf-A fl/fl
Vegf-A Δ/Δ Ncr1-iCre Tg
D
CD31
Vegf-A fl/fl
Vegf-A Δ/Δ-Ncr1-iCre Tg
100µm
CD31
CD31+cells
100
80
60
40
20
0
*
Vegf-A fl/fl
Vegf-A Δ/Δ Ncr1-iCre Tg
E
A-MuLV
% survival
100
80
60
40
20
0
0
30
60
90
120
150
180
day
Vegf-A fl/fl
Vegf-A Δ/Δ Ncr1-iCre Tg
*
F
Vegf-A fl/fl
Vegf-A Δ/Δ Ncr1-iCre Tg
green: CD31
red: NKp46
100µm
CD31
CD31+ cells
50
40
30
20
10
0
*
NKp46/CD31
ratio
4
3
2
1
0
*
Vegf-A fl/fl
Vegf-A Δ/Δ Ncr1-iCre Tg

Figure 6

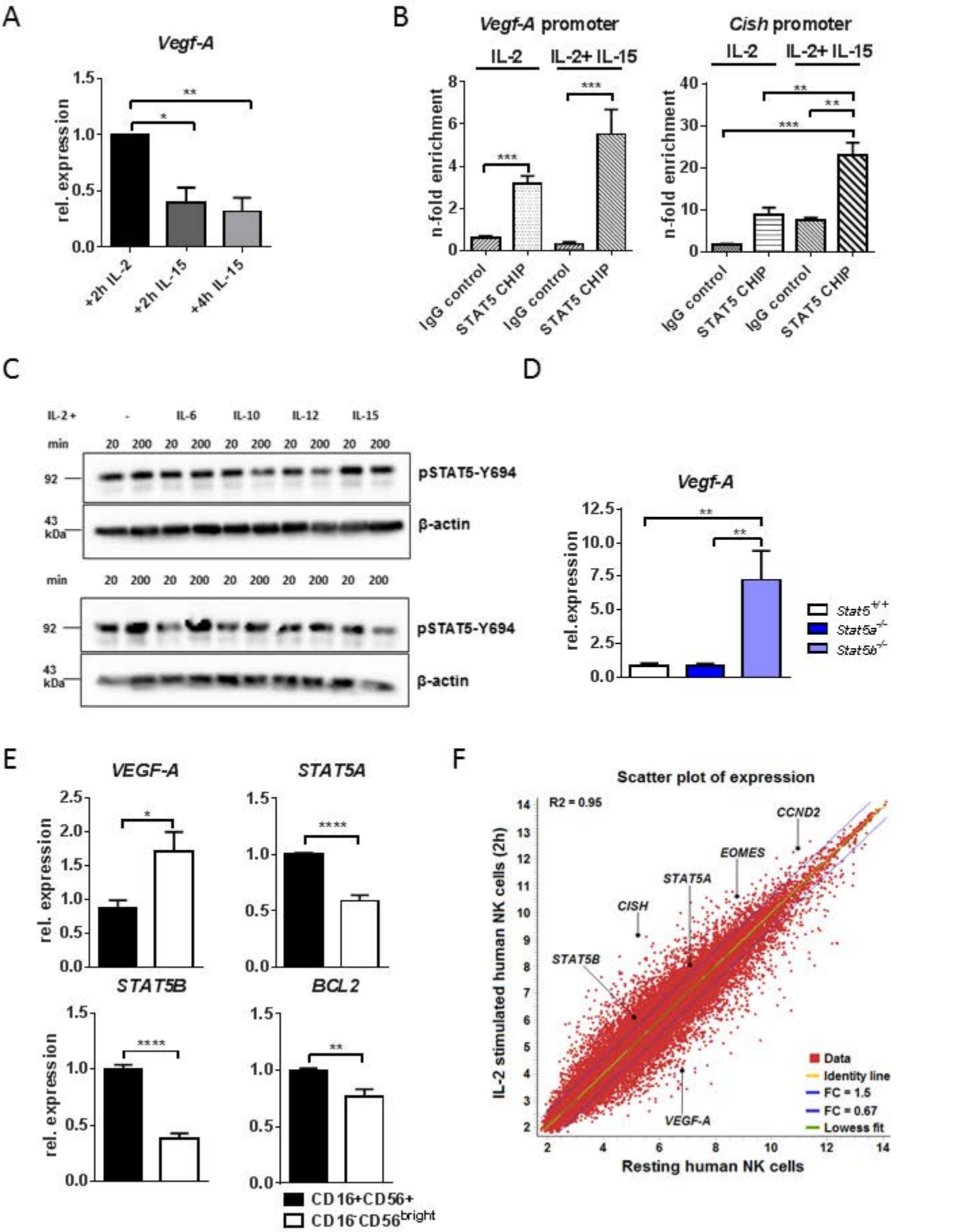
A
Vegf-A
rel. expression
+2h IL-2
+2h IL-15
+4h IL-15
B
Vegf-A promoter
Cish promoter
IL-2
IL-2+ IL-15
n-fold enrichment
IgG control
STAT5 CHIP
C
IL-2 +
IL-6
IL-10
IL-12
IL-15
min
pSTAT5-Y694
β-actin
D
Vegf-A
rel.expression
Stat5+/+
Stat5a-/-
Stat5b-/-
E
VEGF-A
STAT5A
STAT5B
BCL2
CD16+CD56+
CD16-CD56bright
F
Scatter plot of expression
R2 = 0.95
CCND2
EOMES
STAT5A
CISH
STAT5B
VEGF-A
IL-2 stimulated human NK cells (2h)
Resting human NK cells
Data
Identity line
FC = 1.5
FC = 0.67
Lowess fit

Figure 7

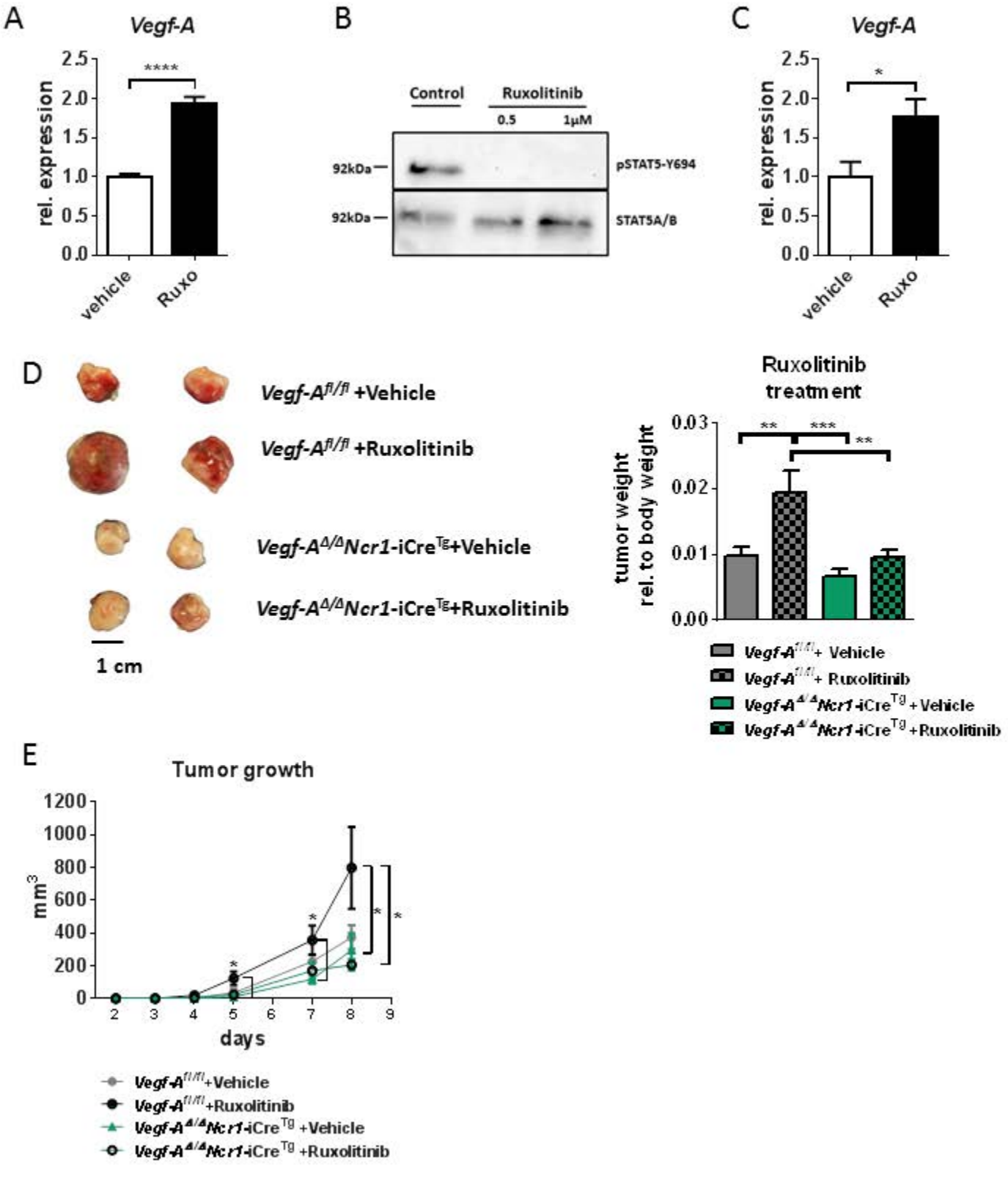
A
Vegf-A
rel. expression
****
vehicle
Ruxo
B
Control
Ruxolitinib
0.5
1µM
92kDa
pSTAT5-Y694
92kDa
STAT5A/B
C
Vegf-A
rel. expression
*
vehicle
Ruxo
D
Vegf-A fl/fl +Vehicle
Vegf-A fl/fl +Ruxolitinib
Vegf-A Δ/Δ Ncr1-iCre Tg +Vehicle
Vegf-A Δ/Δ Ncr1-iCre Tg +Ruxolitinib
1 cm
Ruxolitinib treatment
tumor weight rel. to body weight
Vegf-A fl/fl + Vehicle
Vegf-A fl/fl + Ruxolitinib
Vegf-A Δ/Δ Ncr1-iCre Tg + Vehicle
Vegf-A Δ/Δ Ncr1-iCre Tg +Ruxolitinib
E
Tumor growth
mm3
days
Vegf-A fl/fl +Vehicle
Vegf-A fl/fl +Ruxolitinib
Vegf-A Δ/Δ Ncr1-iCre Tg +Vehicle
Vegf-A Δ/Δ Ncr1-iCre Tg +Ruxolitinib